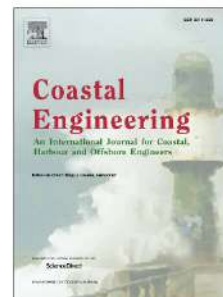# Accepted Manuscript

Survivability assessment of fastnet lighthouse

Alessandro Antonini, Alison Raby, James Mark William Brownjohn, Athanasios Pappas, Dina D'Ayala

Please cite this article as: Antonini, A., Raby, A., Brownjohn, J.M.W., Pappas, A., D'Ayala, D., Survivability assessment of fastnet lighthouse, *Coastal Engineering* (2019), doi: https://doi.org/10.1016/j.coastaleng.2019.03.007.

SURVIVABILITY ASSESSMENT OF FASTNET LIGHTHOUSE

Alessandro Antonini

Assistant Professor of Coastal Structures, Delft University of Technology, NL.

Alison Raby

Professor of Environmental Fluid Mechanics, University of Plymouth, UK

James Mark William Brownjohn

Professor of Structural Dynamics, University of Exeter, UK

Athanasios Pappas

Research Fellow, University College London, UK

Dina D'Ayala

Professor of Structural Engineering, University College London, UK

Contact author: Alessandro Antonini

University of Plymouth
Reynolds Building, Plymouth PL4 8AA
E-mail: Alessandro.antonini@plymouth.ac.uk
Tel: 01752-586124

ABSTRACT

Historic rock lighthouses are unusual structures that are situated in hostile marine environments to provide warning to mariners. Even in an era of satellite navigation their role continues to be an important one, but their survivability into the future is not assured. Out of concern for their ongoing service, the multidisciplinary STORMLAMP project is assessing their survivability under wave loading. This paper presents the various stages of investigations into the structural integrity and stability assessment of the Fastnet lighthouse, situated just off the coast of Ireland. The paper describes: Extreme Bayesian analysis to quantify waves of particular return periods resulting in a 1 in 250 year return period wave with $H_{0.1\%}$ of 17.6 m and an associated maximum force of 20,765 kN; logistically challenging field modal tests revealing the key modal parameters, like the modal masses of 1822 t and 1675 t for 4.8 Hz and 5.0 Hz modes respectively, the cantilevered nature of the overall lighthouse and the directional effects due to the asymmetric contact with the granite rock; and details of a discontinuous finite element model that is used to determine the stability of the tower under the 1 in 250 year return period breaking wave condition, which is well within stability and material strength limits, causing maximum horizontal displacements in the order of 1 mm at the top of the tower. The overall assessment is that the sheer mass of the lighthouse and its interconnected joints are able to withstand the worst of the Atlantic storms.

1. INTRODUCTION

As an island trading nation experiencing some of the world's strongest storms, the UK and Ireland are particularly vulnerable to maritime navigation failure, and loss of one strategic lighthouse will have an incalculable effect on safety, trade and heritage. Historic rock-mounted lighthouses play a vital role in the safe navigation around perilous reefs, however their longevity is threatened by the battering of waves. For a number of years, a consortium of British universities has been investigating the response of rock lighthouses to wave loading. These rock lighthouse structures are built offshore on rocky outcrops to provide navigational information for mariners. Concern had been expressed by the UK General Lighthouse Authorities (GLAs) regarding anecdotal accounts of vibrations on the lighthouses during storms. Whilst all lighthouses are now automated, they still provide accommodation for maintenance engineers on short deployments. Furthermore, the UK GLAs are committed to keeping these physical aids to navigation for future use, as satellite systems are not failsafe and there is concern that storm activity may be increasing with climate change, potentially exacerbating any problems.

Amongst the eight rock towers that are being investigated in the STORMLAMP project there is none more physically significant than the Irish Lights' Fastnet Rock lighthouse in terms of its size and situation. This rock tower is the largest lighthouse in Great Britain and Ireland, with a maximum diameter of 15.8 m and a height of 54 m, with a light at 49 m above Mean High Water Spring, Morrisey, 2005. It is situated on Carraig Aonair, a small islet whose Irish name translates as 'lonely rock', some 4.5 miles off the southernmost tip of Ireland at Cape Clear. This location means that it is the first (or last) structure to be seen on Atlantic crossings to/from Ireland. The rock has a diminutive companion, Little Fastnet, just 10 metres away, separated by a channel.

This paper describes for the first time the adopted multidisciplinary approach to perform the survivability assessment of an offshore lighthouse. The overall aim is the evaluation of threats to the integrity and stability of the structure that may arise from the impact of breaking waves. Specific objectives comprise: Bayesian extreme analysis to quantify the estimated uncertainty of the design waves; the description of the adopted methodology for complex field modal analysis, as well as the dynamic characteristics of the structure in terms of modal parameters, i.e. natural frequencies, damping ratios, modal shapes and modal masses; and finally a discontinuous finite element model is described and then calibrated, before being subjected to a load associated with the identified breaking wave condition.

2. DESCRIPTION OF THE FASTNET LIGHTHOUSE

The current lighthouse structure on the Fastnet rock was preceded by a cast iron tower built in the mid-19th century, this material being a popular choice, particularly in the Far East e.g. Gap Rock in Hong Kong. However, this first tower did not weather well: bolts tying the vertical joints together corroded significantly (by some 50% at the top storey). There were also reports of significant vibrations when the rock was overwashed, such that on one occasion "*a full cup of coffee was thrown off the table in the top room of the tower*", Scott, 1993. Various methods to strengthen the tower were discussed, including encasing the tower or filling the lower storeys. There were also concerns about the state of the rock itself which is "clay slate", some of the soft strata having been eroded, forming large fissures. There was evidently some debate about whether these fissures should be filled, but concerns were aired that the process might actually increase the loading on the rock. In the end, the engineer James Douglass concluded that only the chasm at the west of the rock required filling, Scott, 1993. He subsequently designed the next lighthouse along the lines of his many other lighthouses in the UK and Sri Lanka. Rather than being situated at the centre of the rock, the new tower would be on the west side, on the hardest rock, directly facing the heaviest seas, Fig. 4. Only the western side of the lower courses would be exposed, the lighthouse essentially being cut into the rock itself. This unusual situation gives the lighthouse an axisymmetric nature. This is slightly compounded by irregular positions of openings and the spiral staircase that runs up through the tower. As with Douglass' other lighthouses, the tower is essentially monolithic, with 89 courses formed from concentric rings, each ring comprising dovetailed blocks, which are then connected vertically to the courses above and below by means of keys. Due to the nature in which the lighthouse clings to the side of the rock, the lower courses only have partial rings, which were built into the prepared rock face. A total of 2,074 blocks, each carefully cut to shape, and weighing 1.8 to 3.1 tonnes were used in the construction of this magnificent tower, giving an overall weight of 4,370 tonnes, Fig. 1.

Fig. 1 Drone image of Fastnet lighthouse collected during the field modal test by Mr. James Bassitt (University of Exeter).

3. METHODS

3.1 Wave data source and site specific wave climate characterization

In this study the sea-state hindcast database ATNE (North East Atlantic) was used as main data source. It is run and managed by Ifremer (https://wwz.ifremer.fr/) which give free open access to the results. The available database covers almost 27 years from 1/1/1990 to 30/08/2017, with the presence of two gaps where no data are available, amounting to some 2.4 % of missing data compared to the total theoretical ones. The gaps occur in the intervals between 30/08/1992 - 31/12/1992 and 30/12/1996 - 30/04/1997. The model domain extends between 25 to 73° N and -30 to 30° E as shown in Fig. 2 with the red area. Due to the large domain dimension the structured grid allows a spatial resolution of 10 min. The model is based on Wave Watch 3 (WW3) code and is forced with the wind field provided by the ECMWF (European Centre for Medium-Range Weather Forecasts). The default wave model outputs include a large set of global wave parameters, such as significant wave height (H_s), peak period (T_P), mean period (T_m), peak wave direction (D_P) and mean wave direction (D_m) mainly for deep and intermediate water conditions. All these parameters and data sets are saved at each node of the structured computational mesh with a three hour time-step and made available by means of Ifremer's ftp cloud. Thus, considering the extension of the available time series and the location of the Fastnet lighthouse Fig. 2, the ATNE sea-state hindcast database is considered an appropriate data source for the aims of the proposed study.
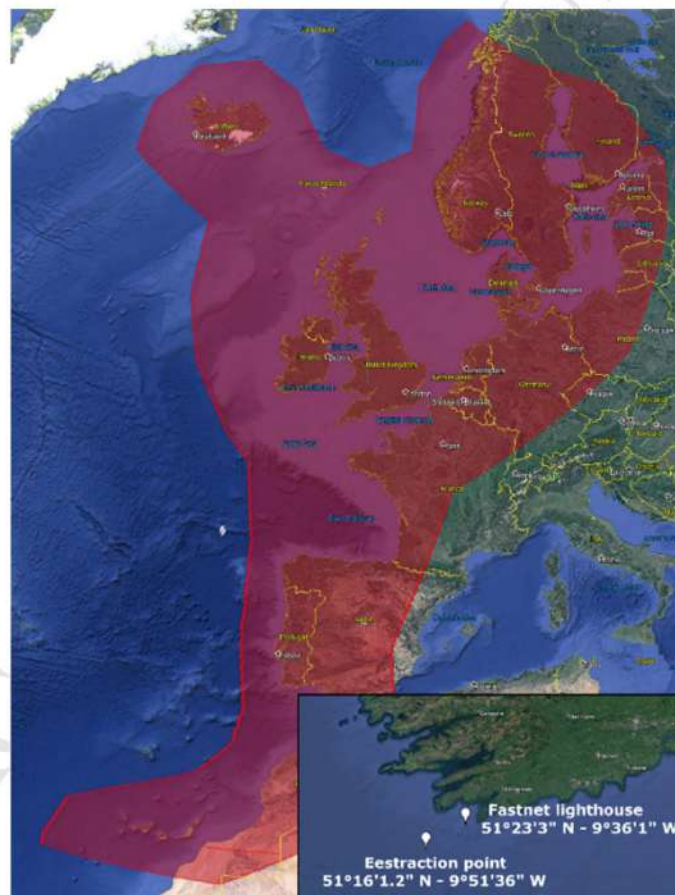

Fig. 2 Ifremer's ATNE numerical model domain (red area), right-lower corner zoom on the location of Fastnet lighthouse and selected extraction point

The wave climate is mainly characterised by an oceanic pattern, the dominant winds blow uninterrupted across hundreds of kilometres of the North Atlantic. In this western area there is effectively no fetch limitation and wave growth is, therefore, duration limited. As it was expected one well-defined directional dominant sector is identifiable ranging between 215 and 290° N. Dominant peak direction[1] is equal to 265° N associated with a sector extended for 75°, (i.e. directional extreme analysis is carried out on data coming from the sector between 215 and 290° N), Fig. 3. Furthermore, the T_P for the largest waves ranges between 12 and 21.3 s, highlighting the swell nature of the events. The maximum H_S was measured on 04/01/1991 at 15:00 and is equal to 14.02 m, with an associated T_P equal to 18.5 s and D_P equal to 274° N. As highlighted in Fig. 4, the combination of the Fastnet rock topography, the location of the structure and the direction of the dominant waves, heavily exposes the lighthouse to the rough action of the waves.
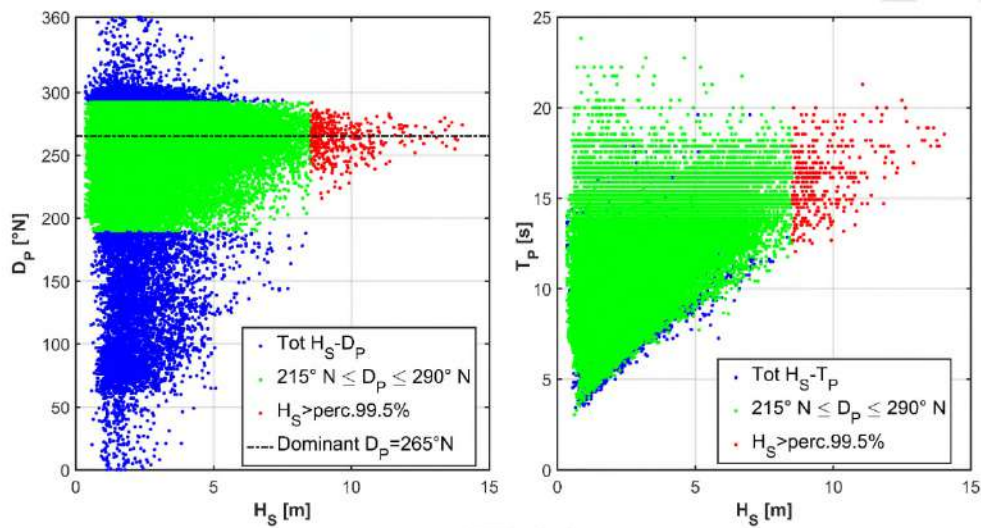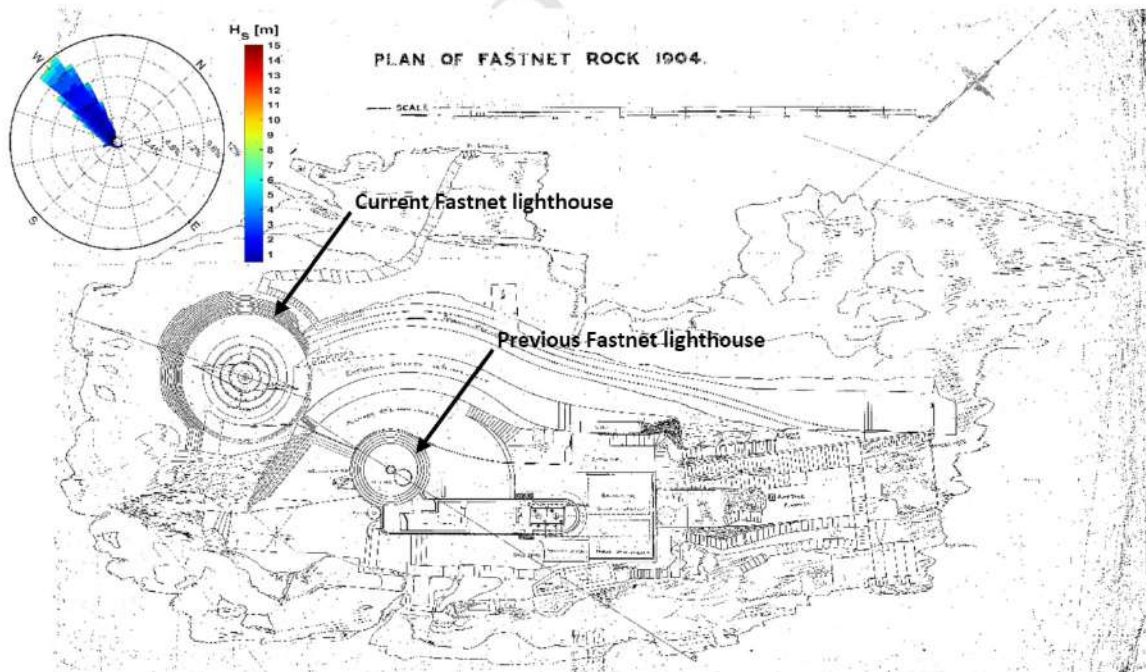

Fig. 3 Fastnet offshore wave climate

3.2 Bayesian extreme analysis & impulsive wave loadings definition

The adopted process leading to the identification of the impulsive wave loading comprises five steps: *i)*, firstly Bayesian inference approach proposed by Cheng et al., (2014), is modified in terms of prior distribution and applied in order to define the return levels. The main finding of this step is a series of posterior distributions for offshore H_S associated with return periods ranging from 2 to 250 years. *ii)*, Secondly, the variation in H_S within the surf zone around Fastnet rock is estimated by means of Goda's (2000) approach, *iii)*, the previous results are adopted as input parameters for estimating the site specific wave heights distribution through the Battjes and Groenendijk's (2000) method. Being the design wave known, *iv)*, the asymmetry between crest and trough at the breaking point is calculated according to the empirical results presented by Hansen (1990). The identification of site specific wave height distribution and wave asymmetry require knowledge of the local bathymetry (i.e. local slope and water depth), which is obtained from archive drawings supplied by the Commissioner of Irish Lights (http://www.irishlights.ie/) and through information available on the INFOMAR website (https://jetstream.gsi.ie/iwdds/map.jsp). *v)*, Finally, the Wienke and Oumeraci's (2005) method is applied in order to define the total horizontal dynamic (*slamming*) load due to plunging wave breaking.

3.2.1   Bayesian inference for extreme wave height analysis

This section describes the adopted statistical framework for estimating return levels of extreme wave heights by means of GPD-Poisson model applied to values greater than a given threshold (i.e. peak over threshold (POT)), using stationary Bayesian inference.

According to Pickands (1975), when the threshold (u) is large, the GPD distribution is defined as in Eq. 1:

$$G_{(y,\sigma,\xi)} = \begin{cases} 1 - \left(1 + \xi\dfrac{y}{\sigma}\right)^{-\frac{1}{\xi}} ; \xi \neq 0 \\ 1 - exp\left(\dfrac{1}{\sigma}\right) ; \xi = 0 \end{cases} \qquad \text{Eq. (1)}$$

where $y = x|_{x>u} - u$ is the exceedance by x of the threshold u, ξ is the shape parameter and σ is the scale parameter. If the number exceedance over a threshold u are assumed to follow a Poisson distribution, with mean event rate λ, the advanced so-called GPD-Poisson model is obtained as proposed by Katz et al. (2002) and Pickands (1975). The model relies on three properties of peaks over the selected threshold: they should occur randomly in time according to the Poisson process, the exceedances should have an approximate GPD distribution and they should be sufficiently far apart to be independent.

In a Poisson process, events are defined as time-points. In this study, events are associated to the storms that are defined as follows. A storm starts when the recorded H_S is greater than the threshold u and has been less than u for at least n consecutive days. It finishes when the recorded H_S is less than u and remains at this level for at least n days. Therefore, the GPD–Poisson model presents the critical problem of selecting the appropriate threshold (u) and minimum declustering time lag (n). Following Coles (2001), threshold selection has been based on the evaluation of the mean residual life trend as a function of a defined threshold range as presented in Fig. 5.a. To select the minimum declustering time lag and check the Poisson character, the dispersion index proposed by Cunnane, (1979), which is the ratio between the variance and the expectation of the number of peaks, is applied and presented in Fig. 5.b. For a Poisson

also an indicator of independence between the data, being one if the data are independent and less than one if there are some dependence. Fig. 5.c shows the analysis undertaken, where the trend for the extremal index calculated for the analysed threshold values (identified with different colours through all the panels) and for the tested declustering time lags (the point highlighted with cross symbol) are presented.
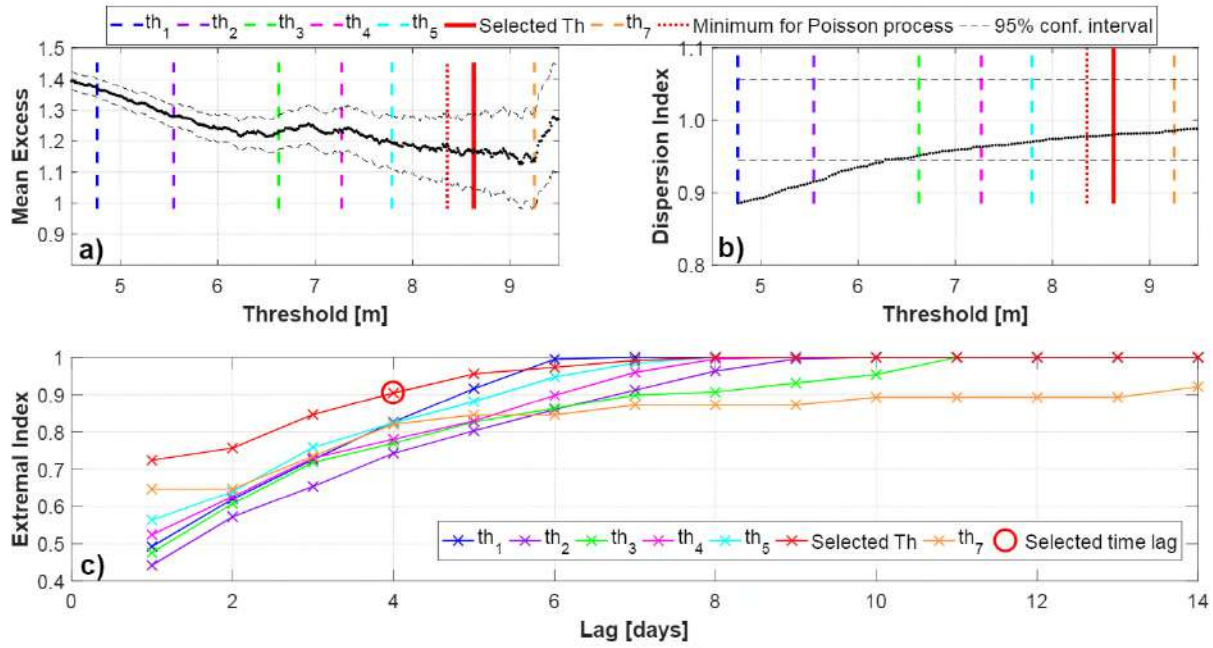

Fig. 5 a), mean residual life plot, 95% confidence intervals based on the approximate normality of sample means, b) dispersion index considering all 7 investigated thresholds and c) extremal index for combination of all seven investigated thresholds and 14 declustering time lags

For the characterisation of the Fastnet lighthouse's offshore wave climate, 7 threshold values are considered, Table 1. Each threshold values is calculated considering the entire directional H_S database shown in Fig. 3, while 14 declustering time lags (i.e. 1 day each) are considered for the sensitivity analysis.

Table 1 Tested threshold values. $\overline{H_S}$ is the mean value of the directional H_S (i.e. H_S for $215 \leq D_P \leq 290°$ N), σ_{H_S} is the standard deviation of the directional H_S, $p_i H_S$ is the ith percentile of the directional H_S

Threshold	Expression	Value [m]	Author
th_1	$\overline{H_S} + 1.4 \cdot \sigma_{H_S}$	4.76	Viselli et al., 2015
th_2	$\overline{H_S} + 1.9 \cdot \sigma_{H_S}$	5.55	Viselli et al., 2015
th_3	$p_{97.5} H_S$	6.63	"
th_4	$\overline{H_S} + 3 \cdot \sigma_{H_S}$	7.27	Arns et al., 2013
th_5	$p_{99} H_S$	7.79	"
Selected	$p_{99.5} H_S$	8.63	Sartini, L. et al., 2015 Méndez et al., 2006
th_7	$p_{99.7} H_S$	9.25	"

Tested threshold values from th_1 to th_3 are too small to properly identify extreme events causing bias. Moreover, they violate the Poisson assumption as the dispersion index is outside the appropriate field of

However, such a choice would violate the Poisson process assumption as highlighted in Fig. 5.b. Moreover, in order to correctly decluster the extremes, a rather long time span would be required (e.g. at least 6 days) leading to a small amount of data and a meaningless "physical" value. Regarding the time span, n is chosen as the optimal compromise between the minimum time interval over which the Poisson process may be assumed to be valid, Luceño et al., 2006, the "physical" time interval to guarantee the independency between consecutive storms, and the length of the time series. Additionally, (not shown for sake of brevity), using the simpler GPD model in Eq. 1, an analysis of the stability of the parameters is carried out. For every value of the threshold u, the parameter estimates have been calculated. As for the mean excess plot, perturbations of the parameters are present for u > 9.1 m. Thus, after inspection of the mentioned plots, we conclude that the smallest threshold values, above the minimum required to respect the Poisson assumption, is adequate for the GPD model. Finally, 8.63 m is selected, corresponding to the 99.5% percentile of the identified directional data. In addition, a time span of 4 days is considered for the declustering process giving an acceptable extremal index equal to 0.905. The stated parameters in turn lead to a dataset of 58 peaks, i.e. with an average value of 2.1 events per year as shown in Fig. 6.
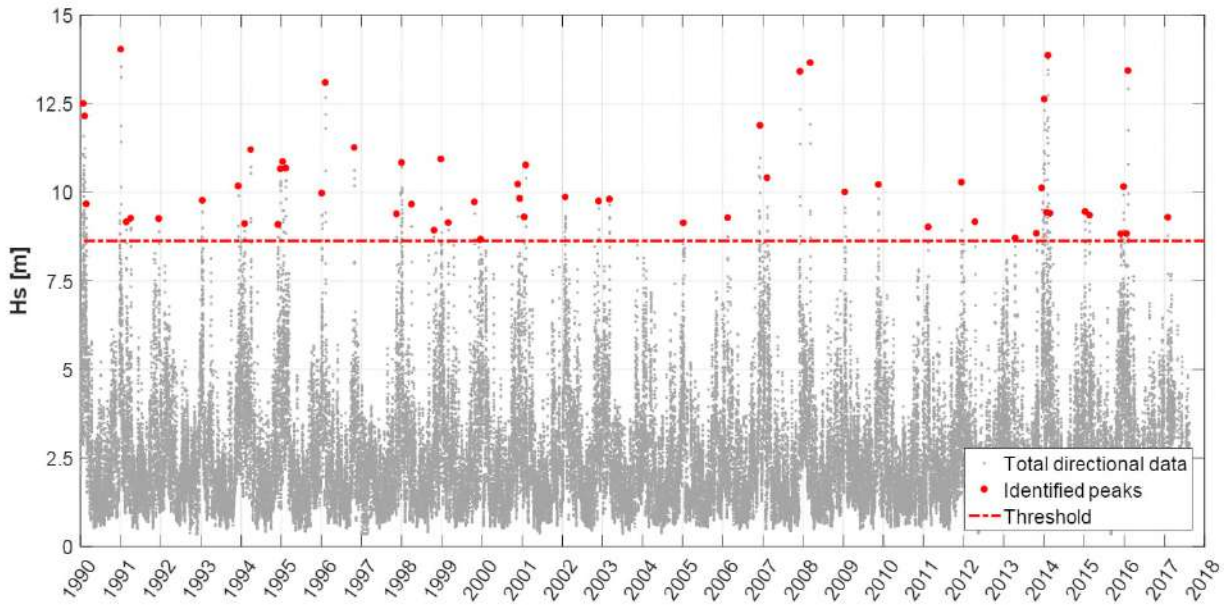

Fig. 6 Total directional data and selected peaks

In this study a Bayesian technique is used to infer the GPD-Poisson distribution parameters as presented by Stephenson and Tawn, (2004). Furthermore, the posterior probability intervals (credible interval) of estimated return levels are provided by combining Differential Evolution Markov Chain (DE-MC) with Bayesian inference according the method proposed by Cheng et al., (2014). This approach combines the knowledge brought by a prior distribution and the observation vector $\boldsymbol{z} = (z_t)_{t=1:N_t}$ into the posterior distribution parameters σ, ξ, where N_t indicates the number of observation, (i.e. the identified storm peaks) in the observation vector $\boldsymbol{z}$. Assuming independence between observations, the Bayes theorem for the estimation of GPD parameters can be expressed as in Eq (2), Coles (2001):

$$\pi(\boldsymbol{\Theta}|\boldsymbol{z}) = \frac{f(\boldsymbol{z}|\boldsymbol{\Theta})\pi(\boldsymbol{\Theta})}{\int f(\boldsymbol{z}|\boldsymbol{\Theta})\pi(\boldsymbol{\Theta})d\boldsymbol{\Theta}} \propto f(\boldsymbol{z}|\boldsymbol{\Theta})\pi(\boldsymbol{\Theta}) = \prod^{N_t} p(z_t|\boldsymbol{\Theta})\pi(\boldsymbol{\Theta}) \qquad \text{Eq. (2)}$$

In order to determine the prior distributions, data at 132 grid points covering the area of south-south-western Ireland around the Fastnet rock, all of them characterised by deep water conditions, have been analysed. The coordinates of the grid points span between 7° to 11.5° longitude West and 50.17° to 51.17° latitude North, the described area being centred on the extraction grid point used to collect the observations. The general assumption is that the parameters vary somewhat smoothly across the region as previously presented by Coles and Powell, (1996), where they consider the problem of estimating extreme wind speeds by defining the prior distribution from an analysis of a number of sites across a region. In the adopted method the idea is to estimate the mean value and standard deviation for the prior normal distributions for the shape and scale parameters from the surrounding grid points. For each of the 132 grid points a classical POT analysis is completed, i.e. the dominant sector and threshold are evaluated, while the time lag is considered the same as that adopted in the extraction point, under the assumption that the storms that generate the events at the extraction point are the same in the surrounding points. Thus, 132 shape and scale parameters comprise the database used to estimate the prior normal distributions. The mean and standard deviation of the prior normal distributions are then calculated considering the weight vector composed of the inverse of the distance between the selected point, among the identified 132 ones, and the extraction point, Table 2.

Table 2 Mean and standard deviation of the prior distributions

	Mean	Standard deviation
Shape parameters	-0.10285	0. 092
Scale parameters	1. 8665	0.229

In Fig. 7 results of the completed POT analysis and classical GPD fitting procedure are presented as a function of location. The black dot identifies the location of the extraction point where the final wave conditions will be provided. The other points show the value of the estimated shape and scale parameters (colour of the points), while the size is proportional to their weight used for the calculation of the mean and standard deviation of the prior distributions. The final results are two normal distributions describing the prior distributions of the shape and scale parameters, Fig. 8. In particular, although the prior mean for ξ is negative, corresponding to a bounded upper tail for the distribution, the prior probability of non-negative values for ξ is non-negligible, being approximately 0.13, so that models for ξ with unbounded right tail are also consistent with the data.
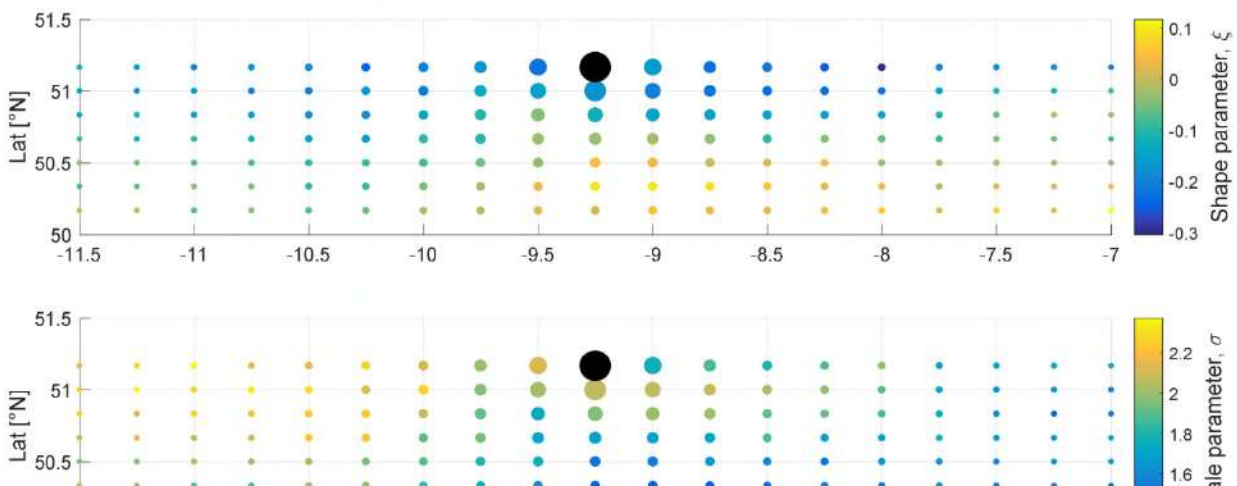
Fig. 7 Upper panel, estimated shape parameters and lower panel estimated scale parameters for each of the 132 grid points. The size of each dot is proportional to the weight used to calculate the mean and standard deviations of the prior distribution. The black dot identifies the extraction point.
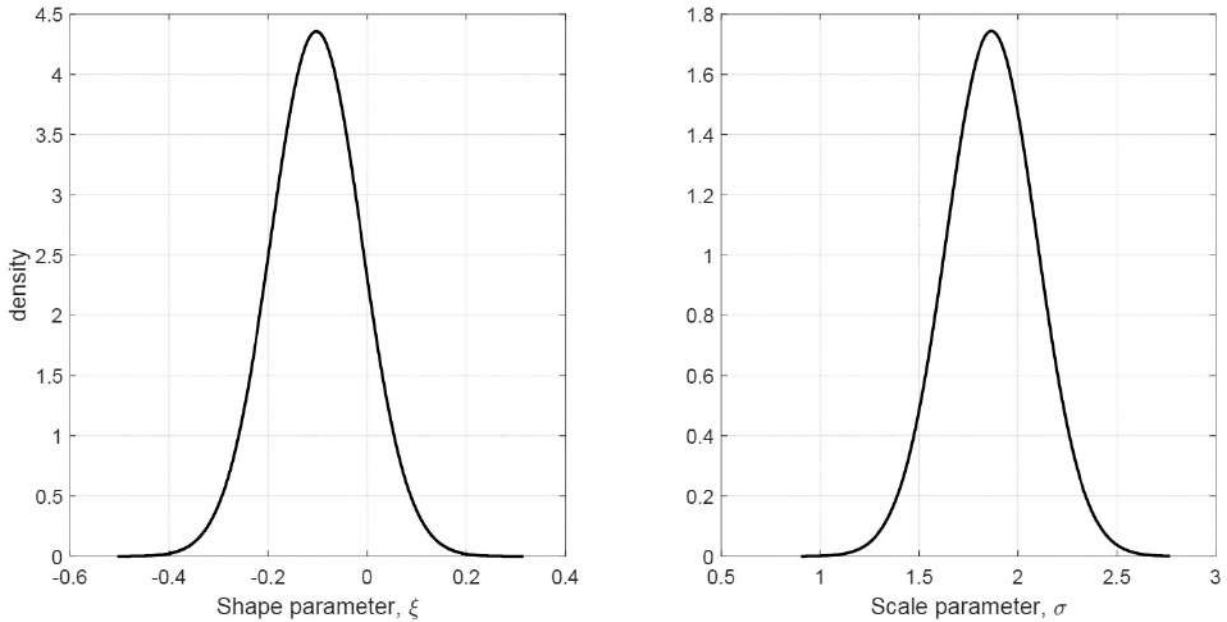

Fig. 8 Priors for shape and scale parameters

3.2.1.2 Design wave conditions

The inference proceeds by the calculation of the posterior distribution in Eq.(2) via the Differential Evolution Markov Chain Monte Carlo algorithm, (DE-MC), Braak (2006). For all evaluations of the prior and posterior distributions, 10,000 realizations are generated in order to create a random walk in the parameters space which converges to a stationary distribution that is the joint posterior distribution. The DE-MC approach integrates a Differential Evolution algorithm (DE), and the Markov Chain Monte Carlo (MCMC), thus DE-MC is a population MCMC algorithm, in which multiple chains are run in parallel; here we have 10 chains. All chains appear to reach equilibrium within the first 150-200 iterations, however, the considered burn-in period is kept equal to 1,000 iterations, so that subsequent analysis is based on iterations 1,001-10,000, Fig. 9. This means that after the chains have been run for 1,000 realizations (the burn-in period) each subsequent sample within the chain will be distributed approximately as $\pi(\boldsymbol{\theta}|\mathbf{z})$. These samples, then, are used to estimate features of the posterior distribution. The convergence of the sampling approach is statistically evaluated according the potential scale reduction factor proposed by Gelman and Shirley (2011). For each distribution parameter, i.e. scale and shape parameters, the variance of the simulations from each chain is computed (after the first 1,000 have been discarded), and then the average of these within-chain variances is calculated and compared to the variance of all the chains mixed together. The square root of the mixture variance divided by the average within-chain variance is the convergence index, $\hat{R}$. When the convergence is reached, the chains will have mixed so that the distribution of the simulations between and within chains will be identical, and the ratio should be equal to one. For the practice implementation procedure Gelman and Shirley (2011) suggest slightly increasing this limit value up to 1.1 in order to avoid applying an extremely restrictive criteria. The potential scale reduction factor values $\hat{R}$ calculated for the realisation within the DE-MC algorithm are 1.0007 and 1.0003 for the scale and shape parameter, respectively. Moreover, the mixing properties of the DE-MC chains, i.e. how well the chains

(1995) and Scotto and Guedes Soares, (2007), suggested that an acceptance rates of 40% should lead to chains that mix well.
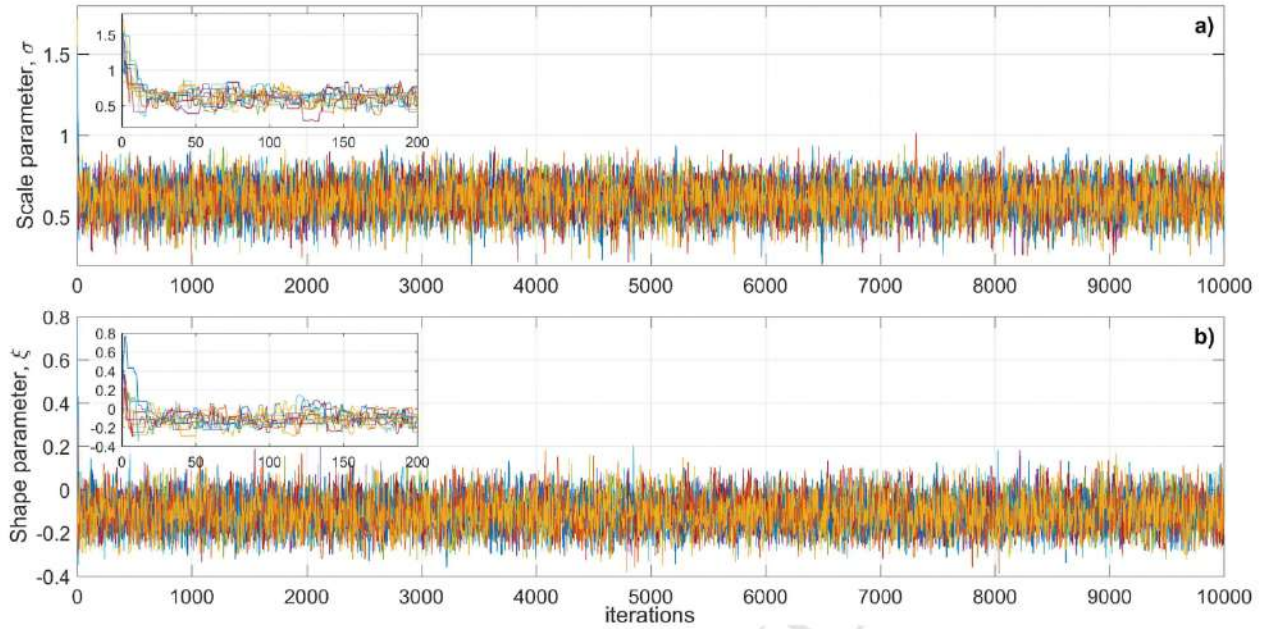

Fig. 9 DE-MC realizations for the GPD parameters σ (panel a) and ξ (panel b), respectively.

The generated ensemble is itself the result of the Bayesian estimation, but it is also the basis to obtain the distribution of hazard parameters, like return level and related credible interval. In the adopted approach, the return levels are expressed as a function of the return period T_R as presented in Eq (3):

$T_R = \dfrac{1}{1-p}$	Eq. (3)

where p is the non-exceedance probability of occurrence in a given year. Moreover, since this study concerns the evaluation of the structure survivability, the design values are required, hence, the most probable values of the ensemble are used as the final return level values, Gibson, 2011, Fig. 10 upper panel. The credible intervals of each computed return level are derived based on 5 % and 95 % posterior probability intervals of the ensemble. Fig. 10 lower panel shows the example of the posterior density distribution related to the 250 years return period, where the return level and the bounds of the credible interval are highlighted.
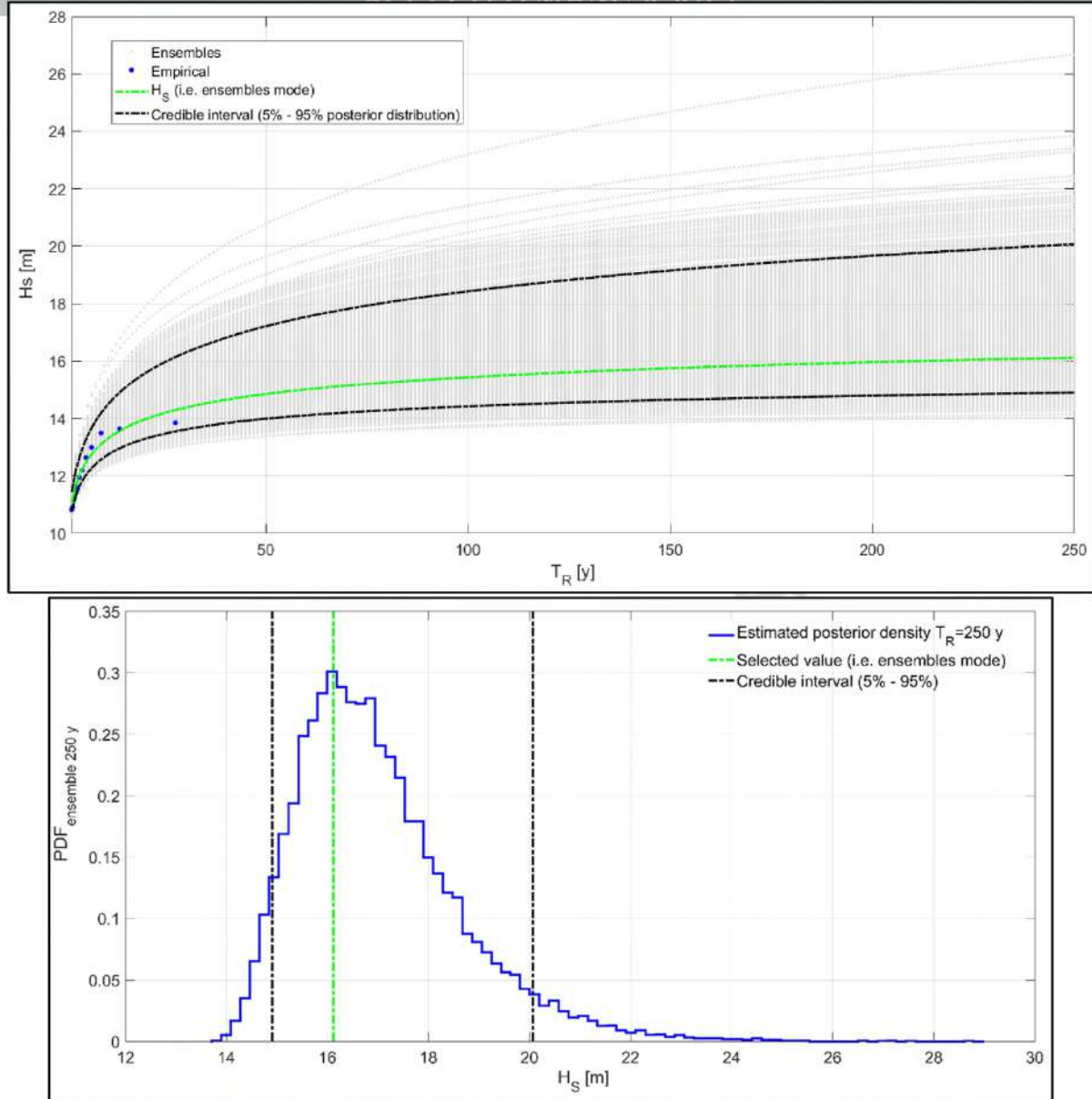
Fig. 10 Upper panel, identified design values and related credible interval. Lower panel, posterior density distribution for return level equal to 250 years.

The peak periods associated with the predicted extreme H_S have been estimated using a linear regression of the measured peak periods versus significant wave heights, see Fig. 11, as proposed by Antonini et al. 2017, Schweizer et al., 2016 and Viselli et al. 2015. A three-parameter power law fit has been selected, based on R^2 comparison results obtained between a three-parameter and the two-parameter law proposed in Det Norske Veritas, 2010 as shown in Eq. (4):

$$T_P = a \cdot H_S^b + c \qquad \text{Eq. (4)}$$

where the parameters a, b and c are equal to -107.5 (-720.1, 505.1), -1.04 (-5.07, 2.99) and 25.9 (-8.84, 60.64), respectively. The values in parentheses indicate 95% lower and upper bounds parameters estimation.
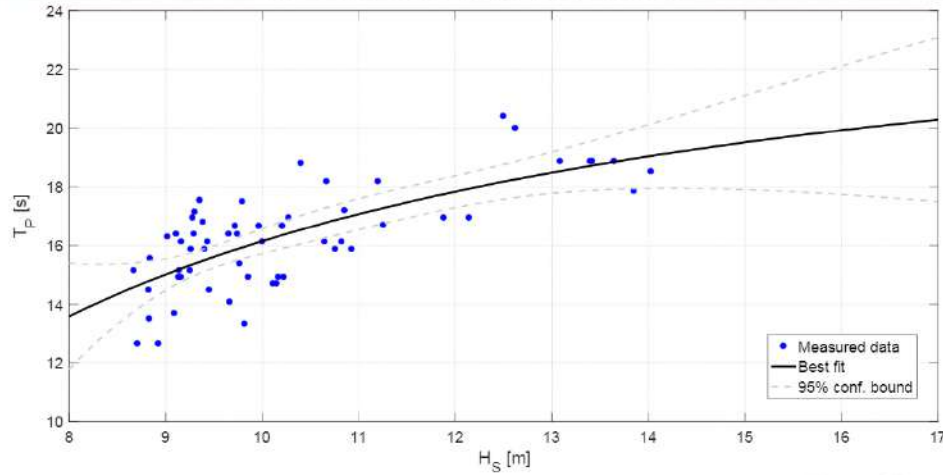
Fig. 11 H_S vs T_P scatter plot and linear regression result for power law function used to define peak period values associated with the extreme H_S.

The final result of the extreme wave analysis procedure is a set of wave states to be used during the survivability assessment of the lighthouse, as summarised in Table 3.

Table 3 Selected wave states for survivability assessment

T_R [y]	H_S (95% cred. inter.) [m]	T_P (95% conf. bound) [s]	D_P [°N]
10	12.95 *(12.65 - 14.33)*	18.45 *(17.76 - 19.13)*	265
50	14.65 *(13.98 - 17.17)*	19.35 *(17.94 - 20.76)*	265
100	15.29 *(14.43 - 18.39)*	19.65 *(17.87 - 21.40)*	265
150	15.64 *(14.65 - 19.09)*	19.80 *(17.81 - 21.74)*	265
200	15.87 *(14.80 - 19.61)*	19.90 *(17.77 - 21.98)*	265
250	16.05 *(14.90 - 20.01)*	19.95 *(17.73 - 22.16)*	265

3.2.2 Impulsive wave loadings definition

Although several studies have been carried out on breaking wave loadings on cylindrical structures installed in deep and intermediate water, a literature review shows the scarcity of results related to cylindrical structures installed above the mean water level, as it is the case for rock lighthouses. In the absence of any other appropriate guidance, and the urgent need to perform a survivability assessment of these ancient structures, Wienke and Oumeraci's (2005) method has been used to describe impulsive wave load. Moreover, a recent study used a similar approach to describe the slamming load due to a real wave impact on the Eddystone lighthouse, Trinh et al. (2016), where the findings showed that the method is a reasonable procedure to describe breaking wave load on a rock lighthouse. Through the present work the quasi-static load is neglected since lighthouses are characterised by high values of natural frequencies as shown in Brownjohn et al. (2018), thus, a slowly varying load as the quasi-static one, does not affect the final dynamic response of the structure. In order to apply Wienke and Oumeraci's method, the wave crest elevation at the breaking point need to be identified, as will be presented next.
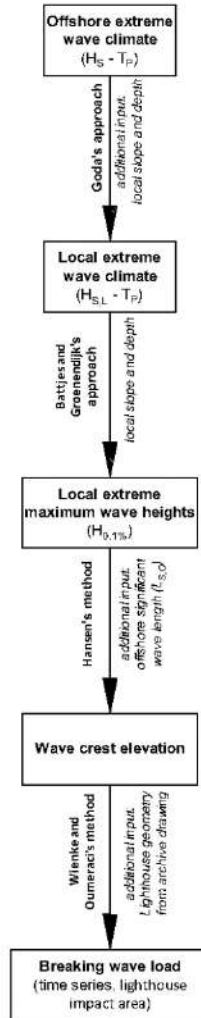
Offshore extreme wave climate (H_S - T_P)

Goda's approach
additional input: local slope and depth

Local extreme wave climate ($H_{S,L}$ - T_P)

Battjes and Groenendijk's approach
local slope and depth

Local extreme maximum wave heights ($H_{0.1\%}$)

Hansen's method
additional input: offshore significant wave length ($L_{s,o}$)

Wave crest elevation

Wienke and Oumeraci's method
additional input: Lighthouse geometry from archive drawing

Breaking wave load (time series, lighthouse impact area)

Fig. 12 Summary of the process leading to the breaking wave load description.

From the offshore extreme wave climate defined above, the significant wave height at Fastnet rock location ($H_{S,L}$) is estimated by means of Goda's approach. The required data, i.e. local sea bed slope and water depth are collected from the INFOMAR website (https://jetstream.gsi.ie/iwdds/map.jsp) resulting in values equal to 1/10 and 10 m, respectively. The effects of the restricted depth-to-height ratio and of breaking wave on the maximum wave height are considered by means of Battjes and Groenendijk's method, therefore, the design breaking wave height is assumed to be $H_{0.1\%}$. Finally, the crest elevation with respect to the still water level (η_b), is calculated according to Hansen's method. Wienke and Oumeraci's method is, then, applied considering the variation of the lighthouse radius within the impact area. The process is summarised in Fig. 12. According to Wienke and Oumeraci (2005) the load distribution is spatially uniform for both the horizontal and vertical direction, while the frontal area affected by the load distribution is between ±30° with respect to the selected wave direction as shown in Fig. 23. The resulting horizontal load time history as well as the affected lighthouse area is presented in Fig. 13 for the 250 year return period wave height.
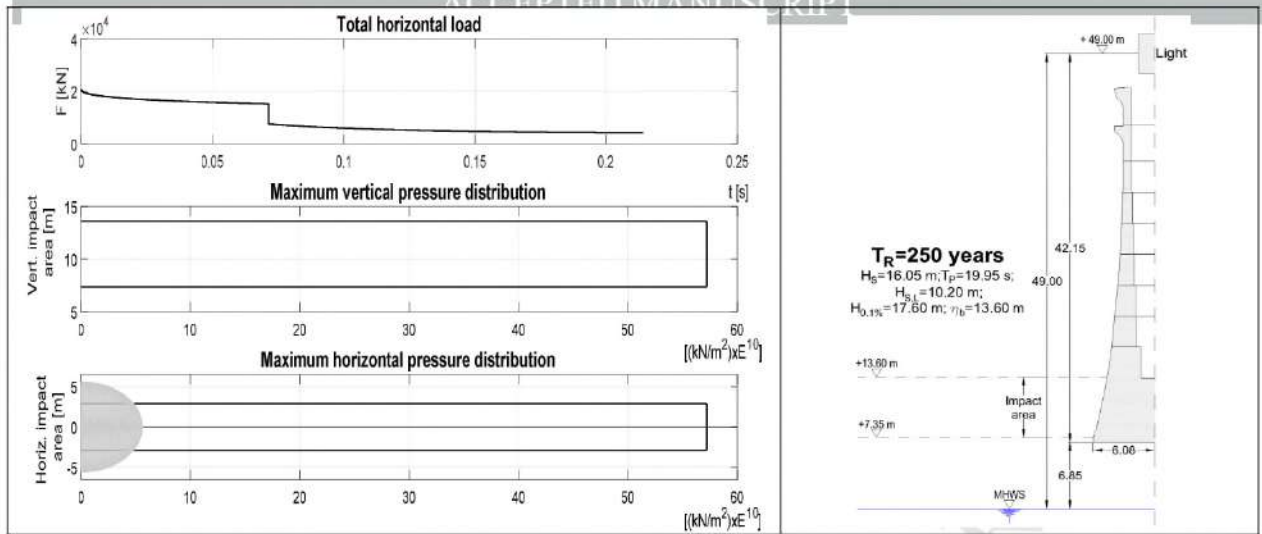
Fig. 13 250 year wave breaking load. Left upper panel: total load time series; left central panel: vertical pressure distribution; left bottom panel, horizontal pressure distribution. Right panel: impact area

The final result of the whole process is a set of wave characteristics describing the design wave climate at Fastnet rock location, the average radius used in the load prediction and the upper and lower points describing the vertical extension of the lighthouse area affected by the wave impact, Table 4. Furthermore, the maximum calculated horizontal load is presented in the last column of the table. Results highlight two important aspects related to the Fastnet rock and its interaction with the incident waves: *i)* in proximity of the rock the wave growth is strongly limited by the bathymetry and *ii)* the green water of the wave crests only impacts the lower courses of the lighthouse, even for the largest return period. As a consequence, the survivability assessment is carried out only for the largest return period, i.e. 250 years. It is worth noting that the study is restricted to plunging breakers generated immediately in front of the cylinder, thus considering the maximum possible impact force.

Table 4 Final design wave climate and related load conditions

T_R [y]	H_S [m]	T_P [s]	T_S [s]	$H_{S,L}$ [m]	D_P [°N]	$H_{0.1\%}$ [m]	η_b [m]	Upper [m]	Lower [m]	Radius [m]	Max. hor. load [kN]
10	12.95	18.45	16.33	10.13	265	16.70	12.72	12.70	6.87	5.62	19570
50	14.65	19.35	17.12	10.15	265	17.21	13.24	13.25	7.15	5.57	20270
100	15.29	19.65	17.38	10.17	265	17.39	13.41	13.40	7.24	5.55	20500
150	15.64	19.80	17.50	10.18	265	17.49	13.51	13.50	7.29	5.55	20620
200	15.87	19.90	17.59	10.20	265	17.56	13.57	13.57	7.33	5.54	20705
250	16.05	19.95	17.65	10.20	265	17.60	13.60	13.60	7.35	5.53	20765

3.3 Field modal test

The offshore lighthouses, granite masonry structures with a massive lantern on top, represent a singular and unusual chance to study the behaviour of historic structures under wave loading excitation. This section describes the complex process used to characterise the dynamic behaviour, in terms of natural frequencies, damping ratios, modal masses and mode shapes, of such remote structures, based on the operational modal analysis (OMA) as well as experimental modal analysis (EMA). Fastnet's dynamical behaviour was measured for the first time on 5th December 2016, as part of the field modal analysis work

Fig. 14 Sherkin Island, 5th December wind intensity and direction, Met éireann, 2019.

Lighthouses are approximately axisymmetric, causing the natural frequencies to appear as two close modes with quite similar modes shapes in orthogonal directions, and showing a weak alignment with the principal directions strongly affected by structural details that disrupt the axi-symmetry, as already highlighted for several offshore lighthouses by Brownjohn et al., 2018. Fastnet lighthouse is a particular example of this type of structure, as it has a clear asymmetry of the lower granite courses for adapting to the irregular shape of the reef, Fig. 1. Moreover, various external openings for windows and entrance as well as the internal spiral staircase and arrangement for heavy equipment can lead to clear principal directions and related modes shapes alignment.
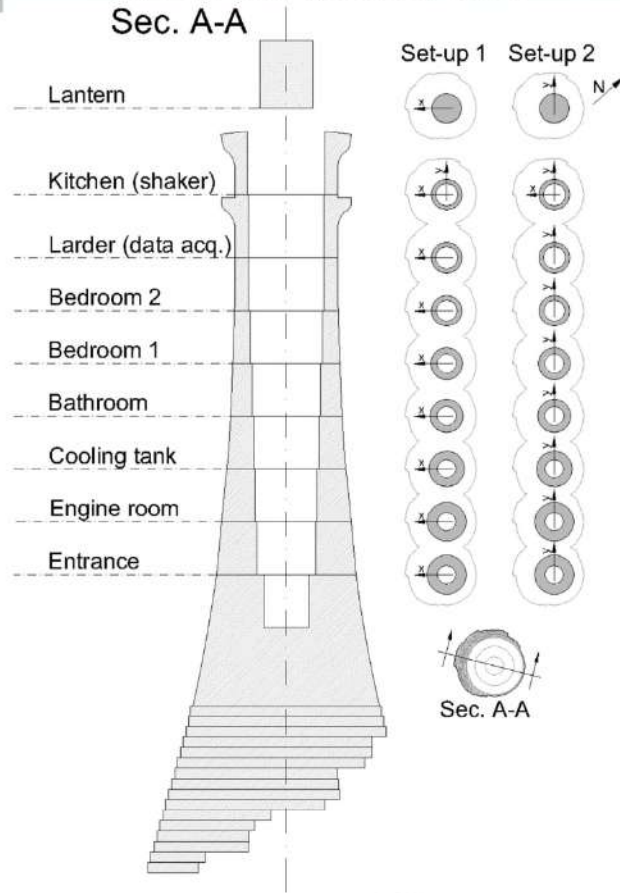
Fig. 15 Layout of the sensors along the lighthouse for both set-up

During the test campaigns, the structural response was recorded by measuring the absolute accelerations at 9 locations, each of them corresponding to a different floor of the lighthouse. Fig. 15 shows a schematic representation of the instrumentation layout, where location of the data acquisition system (larder level) and shaker (kitchen) are highlighted in the upper floors. Furthermore, the adopted alignments for the accelerometers are indicated with the x and y axis, referring to the measurement setup 1 and setup 2, respectively.

For the first of the two accelerometer alignments (setup 1, x alignment), 8 single uniaxial Honeywell QA-750 quartz-flex accelerometers were placed at each of the 8 levels, keeping the same compass bearing with respect to the lighthouse, making use of recurring reference features, while a pair of orthogonal accelerometers was installed in the kitchen. It is worth saying that the accelerometer located in the lantern floor was not measuring the acceleration of the granite body of the lighthouse but the response of the steel structure supporting the lantern apparatus. The x-direction was positive in the south-west direction and y was positive in the north-west direction as shown in the planar lighthouse sections presented in Fig. 15, (right side of the figure). For the second alignment (setup 2, y alignment), the accelerometers placed individually were rotated by 90° clockwise, measuring now along the y-direction. The accelerometers in the kitchen remained as they were. For each setup, the plan was for a minimum of two measurements: one ambient response with no shaker action and one with low frequency (i.e. 3-10 Hz) forced vibration as presented in Table 5. This idea of plan mainly derives from the previous authors' experiences on the field

the possibility of some disturbance of the accelerometers or vibration due to people moving up and down along the lighthouse was very high, so, a preliminary check of the collected data was essential in order to identify the main features of each record as well as its usable part. The main results of this preliminary check of the data are summarised in Table 5Table 5's rightmost column.

Table 5 Measurement sequence

Run	Setup	Shaker direction	Excitation	Duration [s]	comment
2	1	x	Swept sine 3-10 Hz	375	Impulses in channel 2 and 3
6	1	x	Swept sine 3-7 Hz	512	Good data
20	1	x	Swept sine 3-8 Hz	311	Shaker moved
21	1	-	Ambient	1975	Good data
1	2	y	Swept sine 4-6 Hz	440	Good data
3	2	-	Ambient	1592	Good data until 25 frames
4	2	-	Ambient	1720	Good data
5	2	y	Swept sine 5-8 Hz	183	Good data
6	2	-	Ambient	31927	Good data

Unfortunately, the 52 kg APS 113 shaker had problems in the internal electromechanical engine and only worked for a short period of time. Therefore the forced vibration tests analysis relies only on short time series, but still sufficient to identify the lower modes and related modal masses.
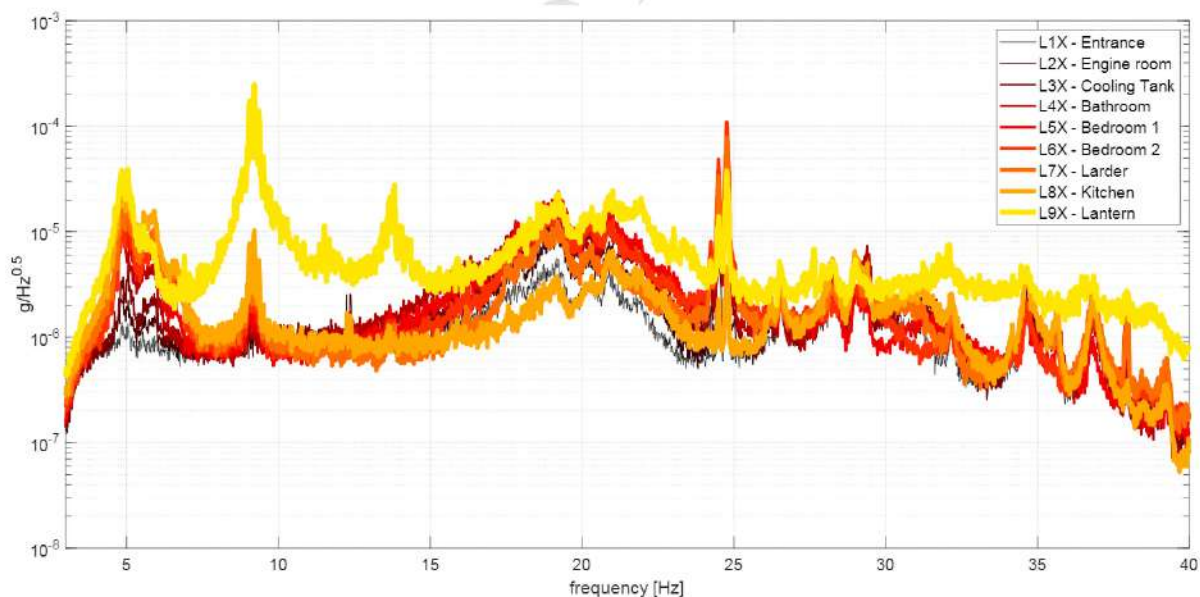

Fig. 16 Auto spectra Run 21, setup 1

The auto spectra in Fig. 16 is an example of the ambient response for the 9 floors in the x-direction, giving

large peak around 9 Hz is mainly driven by the response of the lantern. In contrast, the lantern peak around 13 Hz is not effective in driving oscillations along the main body of the lighthouse. Large widespread energy concentration between 19 and 21 Hz might represent two close structural modes, possibly along different directions. Fastnet lighthouse is powered by means of an electrical generator, resulting in a combination of mechanical and electrical noise in the response data around 25 Hz. Furthermore, at this frequency, the strength of the signal varies between the floors indicating a non-resonant response to the mechanical excitation as already described by Brownjohn et al., 2018. Finally, high frequency energy concentration is visible around 34.6, 35.6 and 36.8 Hz, for the granite structure indicating the presence of possible different structural modes. Large difference, at least one order of magnitude, is evident (Fig. 16) between the lowest (entrance level) and highest (kitchen level) accelerometers positioned on the granite structure indicating a rigid behaviour of the rock foundation compared to the lighthouse structure.

Due to the peculiar shape of the lower courses of the lighthouse we expect a clear alignment of the principal direction with the geometry of the foundation. In order to detect this behaviour, both *x* and *y* signals, measured at the kitchen level, are used. A classical clockwise rotation matrix, considering different realizations of the angle, is applied to the signals which then progressively undergo frequency analysis. In order to detect the alignments we made use of the integral values of the signals' spectrum for each of the rotation angles. Thus, the minimum value of the spectrum integrals corresponds to the direction characterised by largest value of stiffness, whilst the maximum integral value corresponds to the direction with smallest stiffness. The results presented in Fig. 17 confirm the expectation, showing the importance of the lower courses as well as of the contact surface with the rock for the dynamic behaviour of the structure. The non-perfect orthogonality between the principal directions is due to the irregular location of the windows and the heavy equipment (e.g. water tanks) located along the lighthouse's floors. In fact, orthogonality of mode shapes is with respect to mass or stiffness distribution where both are defined at high (strictly infinite) resolution.
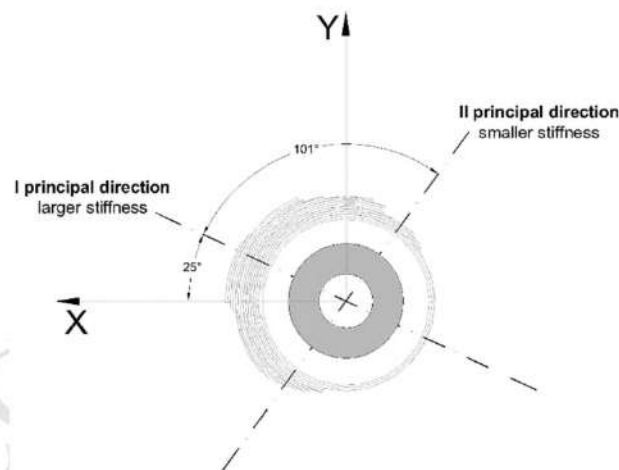

Fig. 17 Top view of the lighthouse. Accelerometers alignments (X and Y) and identified principal directions.

3.3.1 Operational Modal Analysis (OMA)

3.3.1.1 Output only covariance driven stochastic subspace identification

The covariance-driven stochastic subspace identification (SSI-COV) algorithm is, amongst the wide range of techniques available for OMA methods, considered the most robust and accurate, Peeters and De Roeck

Assuming a structure under consideration is being excited by unmeasurable stochastic ambient forces, the discrete time stochastic state-space model is expressed as:

$$\begin{cases} x_{k+1} = Ax_k + w_k \\ y_k = Cx_k + v_k \end{cases}$$ Eq. (5)

where A is the system matrix, C is the output matrix, $x_{(k)}$ and $y_{(k)}$ are the state and observation vectors respectively, where the latter represents the measured signal; $w_{(k)}$ and $v_{(k)}$ represent the statistically uncorrelated Gaussian vectors of the system noise and measurement noise respectively.

SSI-COV starts with creation of a large data matrix T from the response time series assembled as columns of time shifted response $y_{(k)}, y_{(k-1)}$ etc... and whose singular value decomposition leads to an estimation of the A and C matrices. The eigenvalues Λ of A provide the natural frequency and damping ratio estimates while the mode shapes corresponding to measured degrees of freedom are available using C and the eigenvectors Ψ of A as follows:

$$A = \Psi\Lambda\Psi^{-1}$$
$$S = C\Psi$$ Eq. (6)

The A and C matrices are obtained by partitioning T into blocks cutting off at chosen model order, so are not unique. Ranging the model order e.g. between say 10 and 100 and plotting the eigensolution of the resulting states space model in the form of a 'stabilisation diagram' provides a pictorial representation of the quality of the estimation for changing model order. Poles are represented with symbols according to 'stability' of the estimation and superposed on plots of a ambient response auto-power spectral density (e.g. Fig. 16) or the singular values of cross-power spectral density. Fig. 18 shows the stabilization diagram obtained for setup 1 - run 21 by means of MATLAB-based software tool MODAL, Brownjohn et al., 2001. For Fastnet singular value spectra are not used because the capability of singular value decomposition to reveal unique modes is compromised by having only one biaxial measurement in a setup, and in this case the auto-power spectra aid the interpretation of the identification by showing whether or not the masonry tower is participating globally and sensibly in a mode. The symbols indicate that an identified mode is 'stable' in the sense that a set of estimates with consecutive increasing order meet tolerance criteria such as maximum difference of frequency and/or damping between successive estimates, high modal assurance criteria (MAC) between successive estimates and damping estimates being feasible (positive and not above, say 10%).

Seven possible stable poles can be identified. In particular there are stable poles around 5 Hz associated with the first lateral modes of the entire lighthouse (4.9 and 5.7 Hz) as well as one mode mainly related to the lantern mode with the natural frequency of 9 Hz. Despite the results for higher frequencies being more noisy, it is still possible to see other sets of modes. In particular two of them around the widespread energy concentration centred on 20 Hz, more specifically the interested natural frequencies are 18.9 and 20.9 Hz while the remaining ones are identified at 34.9, 35.8, 37.0, 38.0 and 39.2 Hz. As previously stated the energy concentration around 25 Hz is mainly due to the electromechanical noise. It needs to be mentioned that the identified vertical alignments of stable modal properties do not always indicate a secure structural mode; further analysis of the modal shapes combining experimental heuristics and structural behaviour predicted by numerical modelling with experience from other types of cantilevered tower is required to properly assess the dynamics of the Fastnet Lighthouse. In fact experience among the set of rock-mounted lighthouses studied experimentally as part of the STORMLAMP project is supporting new insights into operational modal analysis of axially symmetric structures of this type.
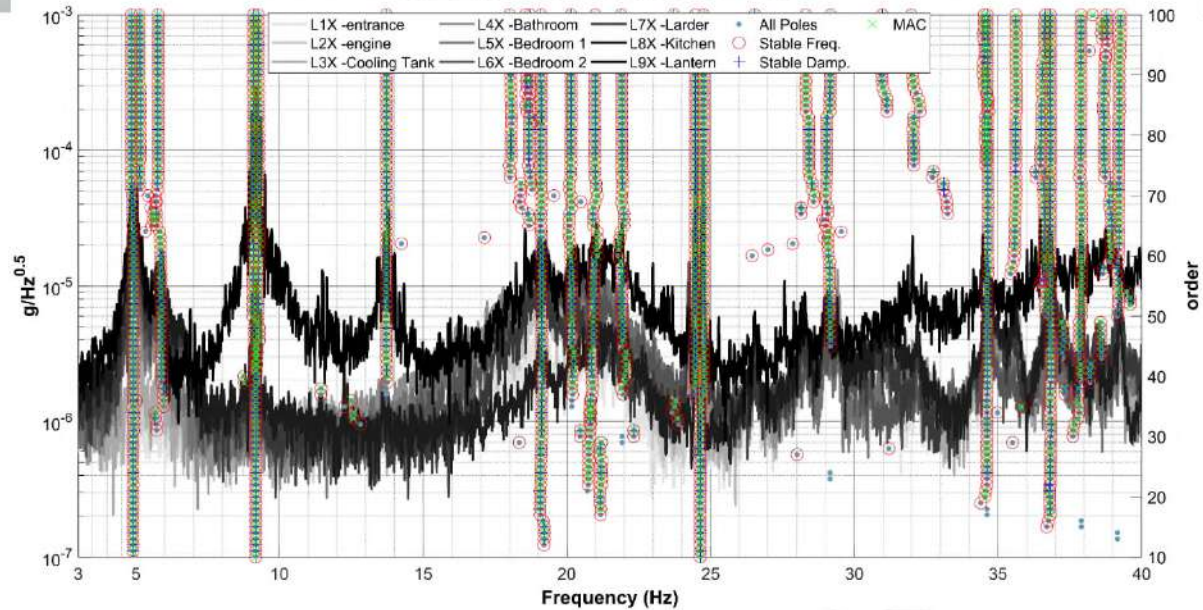
Fig. 18 Stabilization diagram produced by means of SSI-COV Run 21, setup 1

The six mode shapes obtained separately from the two setups are shown in Fig. 22 lower panels. Conventional representation of the mode shapes is adopted in the lower left panel of Fig. 22. The modes are each normalised to unity maximum, then projected onto their own vertical plane which is rotated to an elevation view. Clearly, the pattern of modal ordinate reveals the typical behaviour of a vertical cantilever in both directions.

Having only one floor (kitchen level) equipped with a couple of accelerometers prevent the full analysis on the orientation along the floors by gluing the setups. However, classical SSI-COV analysis is performed for the two signals only at the Kitchen level, aiming to depict the directions of the modal shapes. The detected compass bearing of the modes clearly shows the effect of the directionality of the structure as highlighted by the lower right panel in Fig. 22. It is worth saying that the slightly difference in the identified modal parameters, left and right panels, is due to the different mix of data used in the analysis. So, the identified modes for both vertical (left panel) and planar (right panel) views, are merged according to the similarity of the natural frequencies, generating a full description of the lighthouse dynamic behaviour. The entire set of modes appears to align as orthogonal pairs in which the orientation is mainly affected by the previously described principal directions.

3.3.2 Experimental modal analysis (EMA)

EMA takes advantage of having a controllable and measurable excitation which can be used to generate frequency response functions (FRFs) linking acceleration response to forcing, in the frequency domain. Where a single response measurement is made with forcing at a single fixed point, the approach is termed single input single output (SISO), where there are multiple response points it is termed SIMO and where multiple excitation points used it is termed MIMO. For STORMLAMP, anticipating possible difficulties with acquiring signals of adequate quantity for OMA, the testing program came to use SIMO shaker testing as additional technique to obtain the best quality modal parameter estimates.

usually used to drive a floor/bridge vertically or to drive a footbridge horizontally, in each case the alignment for the shaker being obvious. For lighthouses, a pair of orthogonal directions are chosen arbitrarily, or rather they are aligned with the accelerometer directions which depend on reference features in the lighthouses.

As an example measurement: for setup1, run6, a swept sine excitation was used, ranging from 3 Hz to 7 Hz and back to 3 Hz 4 times over in 512 s. The time series were broken into eight 64 s frames from which cross-power spectra between all signals, both shaker and response, were generated using the Welch procedure Welch, 1967, without windowing or overlap.

The FRF between a response signal for point p and shaker signal (at point q) is obtained using the H_1 estimator:

$$H_{pq}(\omega) = E\left(\ddot{X}_p(\omega)P_q^*(\omega)\right)/E\left(P_q(\omega)P_q^*(\omega)\right)$$

Eq. (7)

where E is expectation (average over the frames).

The FRF is a vector with each component corresponding to a degree of freedom (DOF), which is a unique sensor location and orientation. The FRF for the sensor in the same direction and at the same level as the shaker is termed the *"point mobility"* FRF. EMA of these FRFs used two classical techniques. In this work, the Circle Fit method (Ewins, 2000) was used for preliminary single mode estimates from a single FRF (point mobility) while the Global Rational Fraction Polynomial (GRFP) method was used to obtain the reported modal parameters including mode shape from the complete vector of FRFs for the first two modes. GRFP is implemented in the software ME'scope using a published algorithm (Richardson & Formenti, 1985) that first finds frequency and damping estimates from the ensemble of FRFs over all measurement points, then uses these to identify the scaling factors or residues that contain information on modal mass and mode shape. The rational fraction form is presented in Eq. 8:

$$H(s) = \sum_{k=0}^{m} a_k s^k \Big/ \sum_{k=0}^{u} b_k s^k$$

Eq. (8)

where U is number of modes, $s = j\omega$, $m = 2U$, $n = 2U-1+R$, if U is number of modes and R is the number of residuals accounting for out of range modes. The more recognisable partial fraction form is:

$$H(s) = \sum_{k=0}^{m/2} \frac{r_k}{s - p_k} + \frac{r_k^*}{s - p_k^*}$$

Eq. (9)

where $p = \omega_k \zeta_k + j\omega_k \sqrt{1 - \zeta_k^2}$ and $2\omega_k \sqrt{1 - \zeta_k^2}\, abs(r_k) = \phi_{k,p}\, \phi_{k,q}/m_k$, $\phi_{k,p}$ being the mode shape ordinate for mode k at location p.

GRFP fitting to the setup 1 - run 06 data is shown in Fig. 19. Two modes were assumed for the fit and are clearly indicated, with frequencies 4.8 Hz and 5.0 Hz, with respective damping ratios 1.44% and 1%.
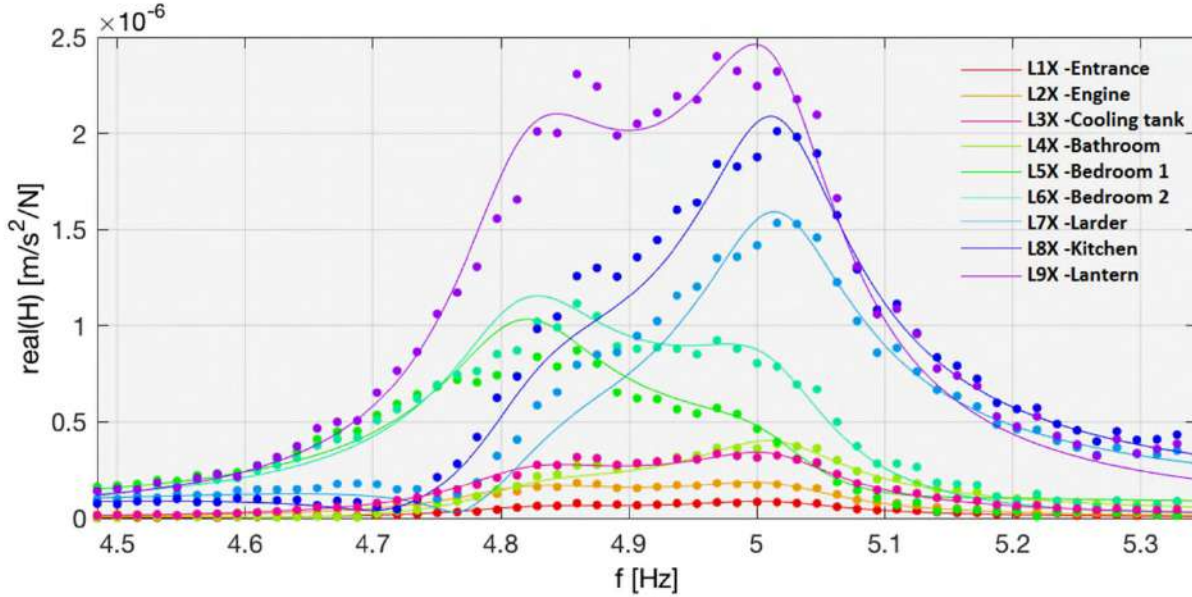
Fig. 19 GRFP curve fit to FRFs from shaking in x-direction (setup 1 - run 06)

The quality of the fit was somewhat compromised due to problems using the shaker that recurred during the field test program of the seven lighthouses in 2016 and 2017, (Brownjohn et al., 2018) and were believed to be due to strong vibrations during the helicopter flights that caused loosening of parts and (twice) destruction of the shaker armature. The greatest difficulties were for Fastnet since the shaker force signal, measured via an accelerometer attached to the armature (of known mass), was corrupted. Although OMA provided more convincing estimation for Fastnet, the benefit of shaker testing is estimation of modal mass, with estimates for 1822 t and 1675 t for 4.8 Hz and 5.0 Hz modes respectively. Because the nominal x and y-directions are rotated with respect to the principal directions and because SSI indicates identical shapes for the two modes, the modal masses along the principal directions can both be taken as the inverse sum of the two individual estimates, hence 872 t.

3.4 Structural numerical modelling

Following the identification of the extreme breaking wave, and the modal properties of the lighthouse, we now consider the structural numerical modelling of the Fastnet lighthouse. This will provide an understanding of the dynamic behaviour as well as stress level of the overall structure under the action of the breaking waves, and thus will provide the final tool to assess the survivability of the lighthouse.

The precise geometry of the Fastnet lighthouse was obtained from archival research on detailed original drawings and photographic material provided by the Irish Lights and the General Lighthouse Authority for Ireland. Moreover, combining the available information provided by Morrisey (2005) about the stone masonry for the original construction together with a catalogued description of the used stones (Watson, 1911), the specific density of the granite has been estimated at 2,645 kg/m³. The on-site inspection and material characterisation confirmed the archival findings, Pappas et al., 2017. The lighthouse comprises a 36.7 m tall granite masonry body and has an 8.3 m high lantern at the top. The diameter of the granite body is 15.8 m at the base and gradually decreases to 6.25 m near the top. The masonry structure consists of 8 vaulted levels, plus the lantern structure on the top. The wall thickness varies between 2.44 m at the

fracture of the dovetailed connections. Sliding, along the horizontal joint between two successive courses of stones, is also blocked by the vertical key connections.

3.4.1 Creation of the FE model and calibration

Based on the geometrical and material information, the numerical model of Fastnet lighthouse is created with the Finite Element (FE) commercial software Abaqus 6.14 (Abaqus, 2014). Research has shown that lighthouse structures of this typology, which are expected to exhibit rocking behaviour due to lack of bonding between horizontal courses, have to be analysed using a discontinuous model (Pappas et al. 2019) to account for the potential opening of horizontal joints during the rocking motion. This approach tackles the limitations of continuous elastic models which, due to unlimited tensile strength and therefore high structural stiffness, considerably underestimate the displacement response.

The FE model consists of 76 full courses of granite stones, whereas the partial courses and the rock foundation are not modelled, under the assumption of fully rigid behaviour of the rock compared to the relatively slender lighthouse. Structured and swept mesh with 8-node reduced integration linear brick elements C3D8R is used. Elastic and homogeneous material properties are assigned to the masonry courses.

The courses are modelled as continuous rings (Fig. 20). The horizontal contact surfaces between the course rings are governed by Coulomb friction law. Due to the very high computational cost, the vertical keying was not explicitly modelled. Therefore, to account for the interlocking behaviour that prohibits sliding between joints, an artificially high coefficient of friction $\mu=5$ is taken. Given the uncertainty about the condition of the joint mortar and its very small thickness with respect to the height of the granite masonry courses, zero cohesion and tensile strength are assigned to the interface for not inhibiting the uplift behaviour. All the courses of the model, including the lowest one, are given the same material and contact properties, and are hence capable of manifesting relative displacements. The adopted material properties and characteristics of the model are summarised in Table 6.
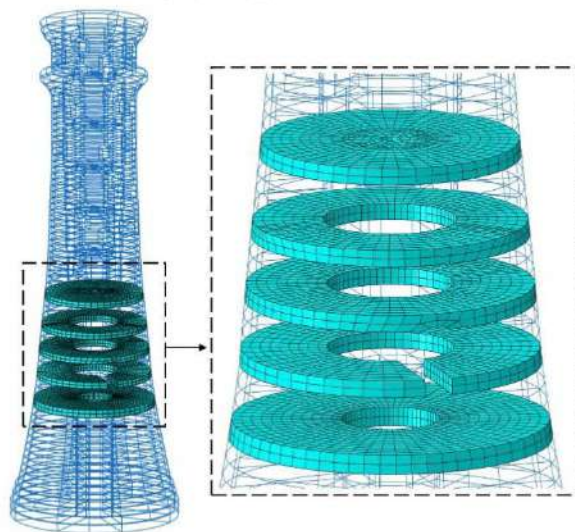

Fig. 20 Fastnet Lighthouse modelled as independent rings without key connections; detail of the 15th, 19th, 23rd, 27th, and 32nd course.

higher stiffness in one direction. This is attributed to the contact with the lateral rock mass which serves as a basement of the entrance for the lighthouse on the north-east side (Fig. 21c). In order to model this constraining effect, lateral spring connections perpendicular to the contact surface are introduced. After sensitivity analysis, the total stiffness of the springs, distributed across 328 elements, is taken to be $2.46 \cdot 10^{11}$ N/m and acts only in the direction normal to the external face of the lighthouse that is in contact with the natural rock, Fig. 23.a,b.
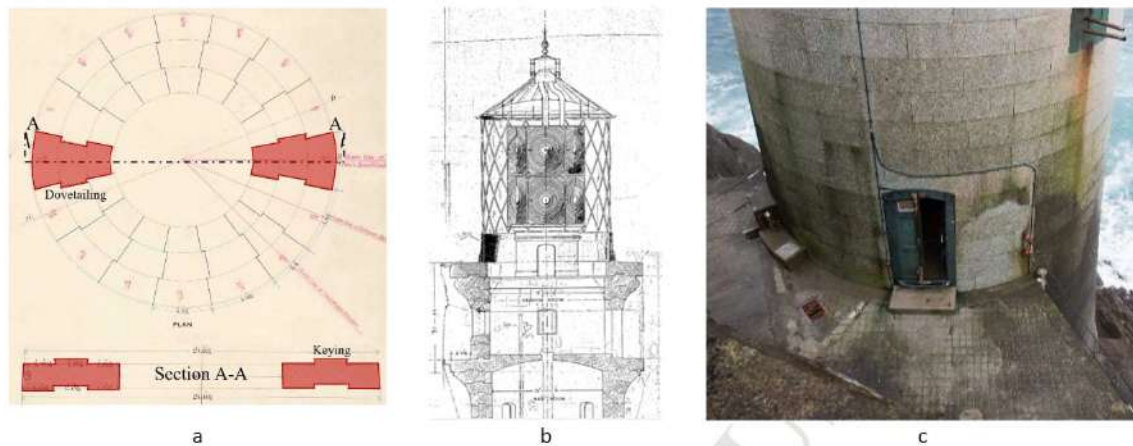

| a | b | c |

Fig. 21 Fastnet lighthouse details: (a) keys and dovetails connection between courses; (b) archival drawing of lantern; and (c) lateral contact with rock near up to the entrance level

Table 6 Numerical material properties and FE model features

FE material properties	
Modulus of elasticity (E)	34 GPa
Material density (d)	2,643 kg/m³
Rayleigh coefficient α	0.6283
Rayleigh coefficient β	$6.366 \cdot 10^{-4}$
Interface type	Friction only
Friction coefficient (μ)	5

The FE model is calibrated on the basis of the on-site experimental dynamic identification results. The results of the numerical modal analysis reveal a very good agreement with experimental values, both in terms of vertical/planar modal shapes as well as in terms of natural frequencies as presented in Fig. 22. Table 7 shows the results of calibration iterations for fitting the numerical results. The modulus of elasticity (E) and the spring stiffness of the rock lateral contact are the variables of this parametric analysis. Because of the orientation of springs parallel to axis x, changes in the stiffness value mainly influence the 2nd, 4th, and 8th modal frequencies. On the contrary, changes of the E value, equally affect all modal frequencies. More details about the influence of independent parameters on the modal frequencies of Fastnet lighthouse can be found in the parametric analysis presented by Pappas et al. (2017).

The final adopted value of the modulus of elasticity is 34 GPa, which corresponds, as expected, to a significantly lower value than the identified one for intact granite (Pappas et al., 2017), mainly due to the discontinuities of the material caused by the horizontal and vertical joints. The directionality of the experimental mode shapes is heavily influenced by the contact with the lateral rock under the entrance door (Fig. 21.c). Thanks to the spring elements that are used to model the interaction with the rock (Fig.

view, while the agreement in term of directionality of the results can be read by comparing the second row of figures and the lower right panel. Moreover, each of the investigated modes resulting from the field modal test is characterised by the colour used in the plot that is also highlighted in the table for the FE results, (e.g. FE 1st mode characterised by a natural frequency equal to 4.85 Hz should be compared with field result having natural frequency equal to 4.8 Hz). Overall the agreement of the results is very good being the maximum difference in term of natural frequencies always smaller than 2.2% and the MAC values always around the unity. Note that the 5th and 6th modes of the FE analysis which are characterised by vertical movement are not identified by the experimental modal tests. Due to the horizontal direction of the wave impact which is not expected to excite these modes of vibration and also because of technical challenges during the on-site campaign (limited space for equipment and short time-frame), vertical measurements were not carried out.

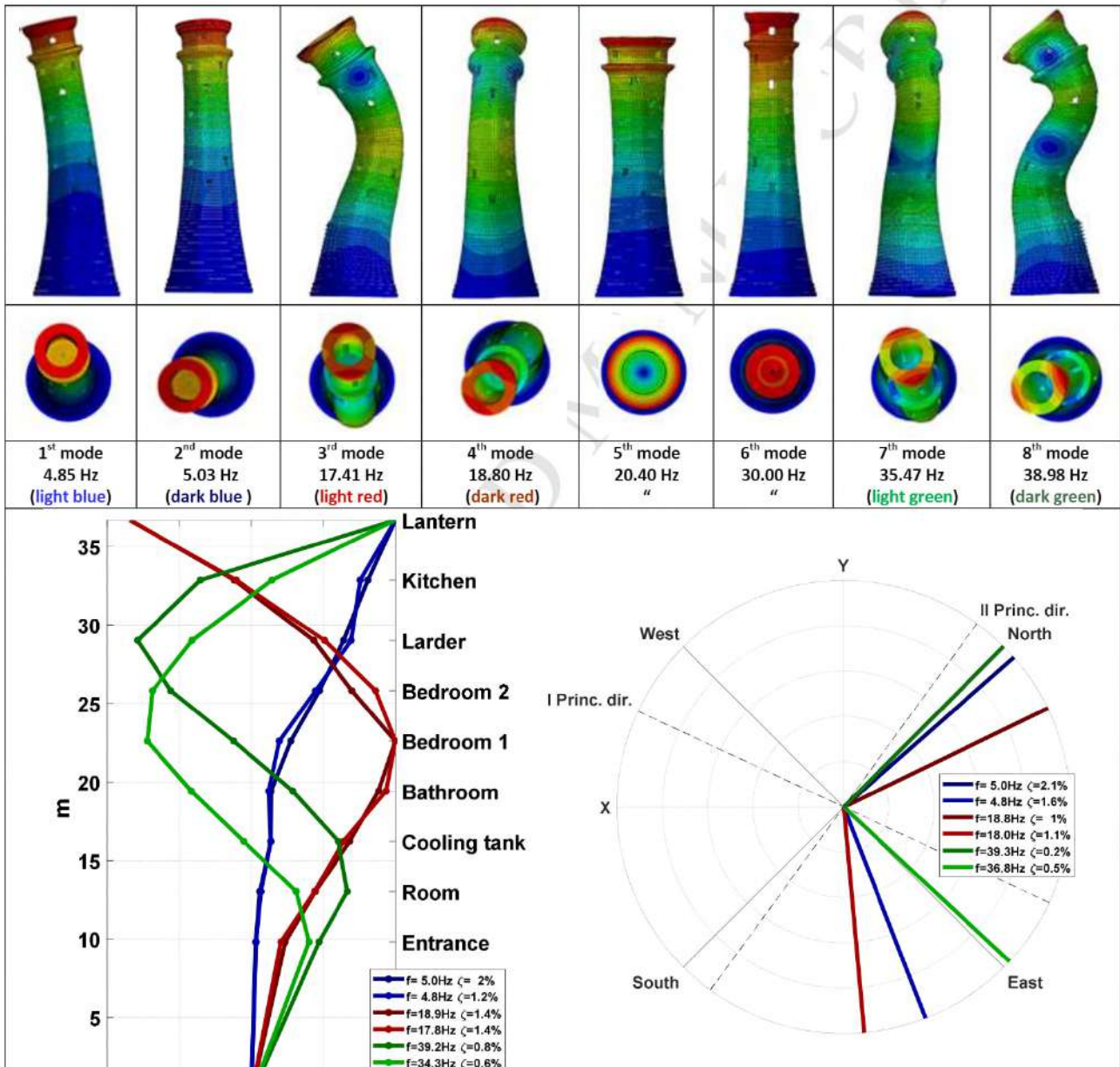| 1st mode 4.85 Hz (light blue) | 2nd mode 5.03 Hz (dark blue) | 3rd mode 17.41 Hz (light red) | 4th mode 18.80 Hz (dark red) | 5th mode 20.40 Hz " | 6th mode 30.00 Hz " | 7th mode 35.47 Hz (light green) | 8th mode 38.98 Hz (dark green) |

Fig. 22 Comparison between the numerical and field modal results. Upper panel FE modal analysis results. Lower panels SSI-COV results. On the lower left panel results for both setups in term of modal shapes projected on a common elevation view, on the lower right panel plan view using only the bidirectional data collected at the kitchen level.

Table 7 Calibration iterations of FE model based on experimental dynamic identification results

		FEM variables		Modes [Hz]							
	Analysis	E [GPa]	Spring total stiff. [N/m]	1st	2nd	3rd	4th	5th	6th	7th	8th
FEM results	#1	34	8.50E+07	4.84	4.85	17.32	17.43	20.30	29.99	35.47	35.89
	#2	34	5.22E+09	4.84	4.86	17.37	17.47	20.30	29.99	35.47	36.07
	#3	34	5.22E+12	4.85	5.14	17.41	19.75	20.54	30.00	35.48	41.28
	#4	34	4.92E+10	4.84	4.93	17.40	17.97	20.33	29.99	35.47	37.13
	#5	**34**	**2.46 E+11**	**4.85**	**5.03**	**17.41**	**18.80**	**20.4**	**30.00**	**35.47**	**38.98**
	#6	36	4.92E+10	4.98	5.07	17.89	18.45	20.92	30.85	36.47	38.12
	#7	35	2.46E+11	4.91	5.10	17.65	19.05	20.70	30.43	35.98	39.50
Experimental results				**4.8**	**5.0**	**17.8**	**18.9**	**-**	**-**	**35.7**	**39.2**

3.4.2 Structural analysis for wave impact

The impulsive force time-history due to the breaking wave is calculated according to the previously described methodology. For the structural analysis, the 250 year return period impulsive wave is used. This wave combines the highest impact height with the strongest impact forces and is therefore the least favourable scenario. Moreover, in order to maximise the response, the impact direction is set at 290° N. This impact direction has the highest eccentricity in respect to the lateral support due to the rock mass Fig. 23.a, and is therefore the worst case impact scenario, at the same time is coherent with the identified possible dominant direction.

The loading conditions, i.e. the total horizontal force time history and the resulting pressure distribution, are described by means of the methodology presented by Wienke and Oumeraci's (2005). The idea is to apply the equilibrium concept and homogenously distribute the pressure so that the integral is equivalent to the total horizontal load previously identified. In this light the definition of the lighthouse area affected by the impact is of fundamental importance. Wienke and Oumeraci, also provide some indications about the interested area. The vertical extension of the affected area can be identified by means of the maximum wave crest (η_b) defined above and the curling factor. The maximum height affected by the wave impact is equal to η_b while, under the hypothesis that the impact takes place simultaneously at each level of the affected area, the lowest point is identified by means of the curling factor, λ. Coefficient λ describes the part of the surface elevation (η_b) of the breaker, which contributes to the impact. The adopted λ value is equal to 0.46 well in agreement with the commonly cited value given by Goda (1966), i.e. λ =0.4–0.5 for plunging breakers. In the analysed case, η_b is equal to 13.60 m above the mean high water springs (equivalent to 6.75 m above the first full course of stones) and the lowest point is equal to $\eta_b \cdot (1- \lambda)$=7.35 m above the mean high water springs, (equivalent to 0.5 m above the first full course of stones). Thus, the load is applied on 11 courses and the force resultant is at a height of 10.475 m above the mean high water springs, (equivalent to 3.625 m above the first full course of stones). On the other hand, the horizontal extension of the affected area is described by means of the evidences presented by Wienke through the

the impact, while the intensity of the pressure is just the result of the ration between the total load presented in Fig. 13 and the mentioned area (assumed to be flat) and shown in Fig. 23.c. The total duration of the impact is 0.215 s, and the maximum impact force, at t = 0, is equal to 20,765 kN. Moreover, the total impulse of the applied load is equal to 1,937.7 kNs. The pressure distribution is taken uniform both in horizontal and vertical directions.
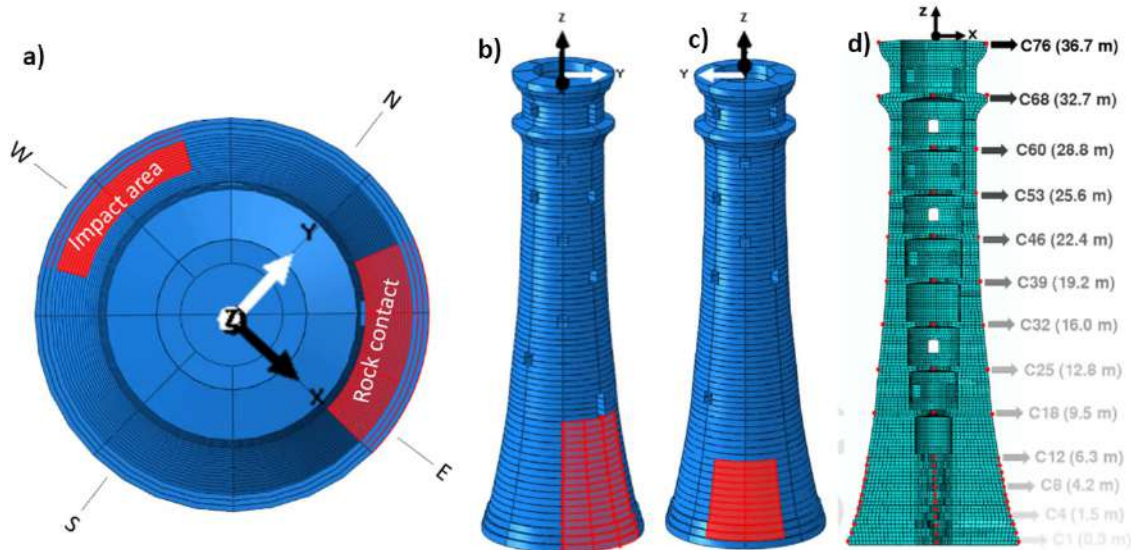

Fig. 23 FE model: (a) top view with impact and lateral contact areas; (b) lateral contact area; (c) impact area; (d) control points at various course levels

The structural response of the Fastnet lighthouse is obtained after FE analysis with Abaqus/Standard using the wave impact time-history with a maximum time-step increment equal to 0.002 s. Although such a small time-step significantly increases the computational cost, it is necessary for capturing the high frequency vibrations of such an intense and short duration impact. Rayleigh damping is adopted for the FE model (coefficients listed in Table 6), with minimum level of damping equal to 2% at 5 Hz.

The structural response of the FE model, in terms of horizontal and vertical displacements, is recorded on the control points shown in Fig. 23.d. The control points are placed on both sides of the structure and on the axis of symmetry. The positive direction for the horizontal displacements is the same as the impact direction and for the vertical displacements is the opposite of the gravitational direction. The graphs of Fig. 24 and Fig. 25 show the horizontal and vertical displacements of the control points at various levels. The response time-history was calculated for a total time of 2.0 s, which includes the highlighted impact duration of 0.215 s and a post-impact free-vibration period with damping. The analysis revealed an intense phase difference of the upper versus the lower control points for the beginning of the motion, represented as dark and light lines, respectively. The higher frequencies, which dominate in the lower and massive courses, are gradually damped out and all areas of the lighthouse pass to an in-phase vibration. This different behaviour of the response highlights the heterogeneous nature of the structure along its development, having a stiffer lower area and a relatively weaker upper zone.
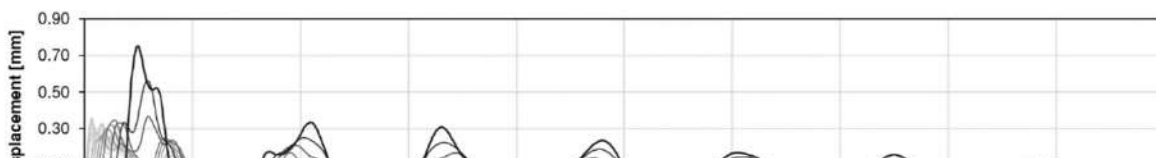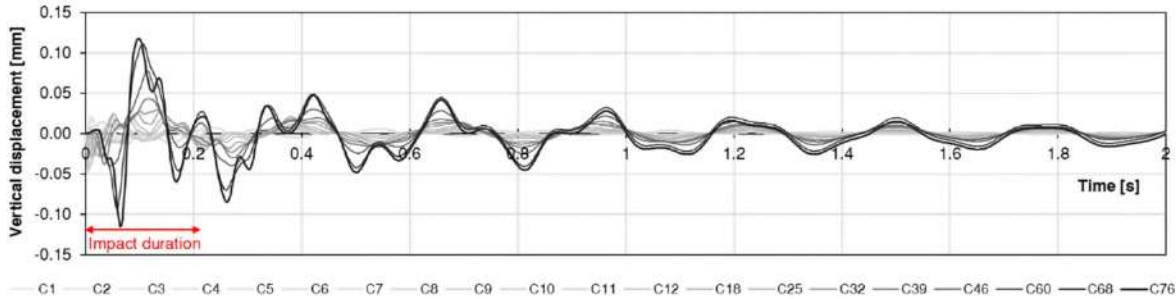
Fig. 25 Vertical displacement at control points on the impact side, lighter lines indicate lower control points.

The maximum amplitude of horizontal displacement is 0.78 mm and is recorded on the top course of the lighthouse at around 0.1 s. Similarly, the maximum amplitude of vertical displacement is 0.12 mm and is found at the same control point and time. These small values of maximum horizontal and vertical displacements reveal a modest structural response suggesting that the lighthouse stability is not jeopardised by the wave impact. Regarding the distribution of stresses in the structure, the numerical analysis for static conditions yields minimum and maximum principal stresses equal to -0.86 MPa and 0.42 MPa respectively, both of which are found near the openings. The maximum stress level during vibration increases to -2.06 MPa and 0.99 MPa for minimum and maximum principal stresses respectively (Fig. 26). These values correspond to levels lower than 2% of the compressive and 18% of the tensile strength of the granite material with which the lighthouse is constructed. Regarding the sliding between the courses, which unlike the uplift and opening of the horizontal joints is not reversible, the numerical analysis did not yield any significant levels of dislocation. However, it is estimated that for a coefficient of friction μ around 0.58, sliding could be possible. Nevertheless, as it was presented earlier, the ingenious design with vertical keys prevents any of such substantial dislocations. These findings suggest that a lone breaking wave generating an impact load of this intensity, duration, and for this impact height, does not pose an imminent threat to the stability of the Fastnet lighthouse.
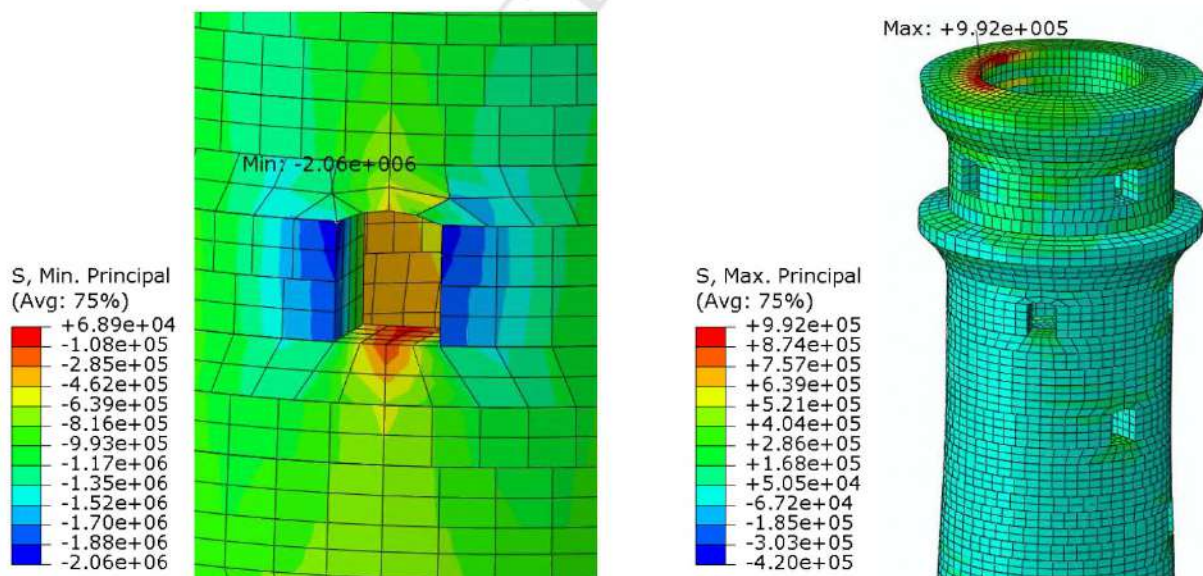

Fig. 26 FE model: Minimum principal stresses at 0.052 s (a); maximum principal stresses at 0.070 s (b)

wave forces act up to the 12th course, whereas the lighthouse has a lateral support up to the 18th course. Therefore, a great portion of the forces is transferred and absorbed by the lateral rock support. Furthermore, the wave impacts the levels below the main entrance which are built as solid courses without any internal voids. This area not only offers better strength against lateral forces thanks to the lack of voids, but also contributes to higher damping due to its high mass and friction along the courses during vibration as highlighted by the different behaviour of the control points displacements presented in Fig. 24 and Fig. 25.

4. CONCLUSIONS

The presented findings arise from the first comprehensive multidisciplinary investigation carried out in the framework of the EPSRC funded project STORMLAMP - STructural behaviour Of Rock Mounted Lighthouses At the Mercy of imPulsive waves. By combining expertise from different fields of engineering, this research addresses, in three different steps, the survivability assessment of the iconic rock mounted Fastnet lighthouse, presenting a promising methodology also for the assessment of other types of coastal structures like caisson breakwaters, crown-walls and more generally all structures characterised by a significant dynamic response under the action of the breaking waves.

The first step involved the identification of the breaking wave load. Based on Ifremer's hindcast database, the Fastnet rock offshore extreme wave climate has been identified by means of Bayesian inference of Generalised Pareto Distribution. The vast amount of available information provided by the hindcast numerical nodes has been considered through the informative priors distribution for the GPD's scale and shape parameters, assuming a prior normal distribution for both parameters. The design wave climate, i.e. punctual value obtained from the posterior distribution, is provided in terms of most probable value, while the credible interval is provided as the 5 and 95 percentiles of the posteriors. Offshore wave climate highlights the severity of the location, presenting significant wave heights up to 16 m for a return periods of 250 years. However, the shallow foreshore nature on which Fastnet lighthouse was built does not allow the development of massive impact, having local significant wave heights only slightly in excess of 10 m due to bottom induced breaking. For the 250 year return period wave, Wienke and Oumeraci's approach applied to extreme wave impact load calculation led to the identification of a corresponding 1,937.7 kNs maximum impulse.

The second main activity of the work involved the dynamic characterization of the lighthouse, based on the measured field data. Although there were logistical difficulties of the modal tests due to the remote location of the lighthouse, the main technical difficulty was identifying the directionality of the modes. An operational modal analysis technique in the form stochastic subspace identification (SSI-COV) and forced vibration test in term of global rational fraction polynomial (GRFP) have been adopted for the identification of the modal parameters such as natural frequencies, modal shapes, damping ratios and modal masses. The identified modes show classical modal shapes of a vertical cantilever, with the first two modes in the range of 4-5 Hz, in close agreement with the previous analysed lighthouses presented by Brownjohn et al., 2018. The symmetry of the lighthouse for the large part of its development, results in pairs of modes in more or less orthogonal directions close to the identified principal directions. However, the identified principal directions are strongly affected by the asymmetry of the lower part of the lighthouse structure, generating a stiffer and weaker direction. For Fastnet this alignment is mainly due to the asymmetric contact with the rock and to the partial lower courses.

creation of an advanced non-continuous FE model that allows separation between the courses of stones as well as the representation of the joints between each stones. To the authors' knowledge, this is the first time that such a modelling approach has been implemented for studying the response of a structure exposed to wave impacts. The structural analysis revealed modest values of maximum horizontal and vertical displacements and also low levels of principal stresses for the impact wave loading due to the 250 years return period wave. Furthermore, the resulting displacements are in the order of magnitude of 1 mm, while the principal stress does not exceed 2% of the compressive and 18% of the granite tensile strength. Moreover, no significant and irreversible sliding between the courses is highlighted by the model, mainly due to the capacity of the dovetails and key connections to resist the horizontal loadings. This suggests that, even though the lighthouse was designed and built more than 100 years ago, the structure is not threatened by the current wave action.

Two elements have been identified as key aspects contributing to the structural stability of the Fastnet lighthouse. First of all is the massive nature of the construction as well as the meticulous construction of the connections between the stones. Secondly is the height of the structure above the s.w.l. that guarantees impact wave loadings acting only on the lower courses, characterised by the absence of internal voids as well as by a solid contact with the basement rocks, thus generating an extremely stiff lower area and consequently modest dynamic response of the whole lighthouse structure.

This investigation shows that stability of the Fastnet lighthouse, in its current condition, gives no cause for concern and its physical presence will continue to provide warnings to mariners long into the future.

5. ACKNOWLEDGEMENTS

6. BIBLIOGRAPHY

Morrissey, James, 2005. A History of the Fastnet Lighthouse. Columba Press; 2nd ed. Edition.

Scott, C.W., 1993. History of the Fastnet Rock lighthouses. Schull Books.

Cheng, L., AghaKouchak, A., Gilleland, E. and Katz, R.W., 2014. Non-stationary extreme value analysis in a changing climate. Climatic Change, 127, pp. 353-369.

Goda, Y. 2000. Random Seas and Design of Maritime Structures, 2nd edition, World Scientifc Publishing Co., Singapore, ISBN-13: 978- 981-4282-39-0, 2000.

Battjes, J. and Groenendijk, H., 2000. Wave height distributions on shallow foreshores, Coastal Engineering, 40, pp. 161-182. DOI: 10.1016/S0378-3839(00)00007-7.

Wienke, J., Oumeraci, H., 2005. Breaking wave impact force on a vertical and inclined slender pile—theoretical and large-scale model investigations. Coastal Engineering, 52, pp. 435-462, DOI:10.1016/j.coastaleng.2004.12.008.

Pickands, J., 1975. Statistical inference using extreme order statistics. Annals of Statistics 3, 119- 131.

Katz, R.W., Parlange, M.B., Naveau, P., 2002. Statistics of extremes in hydrology. Advances in Water Resources, 25, pp. 1287-1304. DOI: 10.1016/S0309-1708(02)00056-8.

Coles, S., 2001. An introduction to statistical modeling of extreme values. Springer series in statistics. Springer.

Cunnane, C., 1979. A note on the Poisson assumption in partial duration series models. Water Resources Research, 15 (2), pp. 489-494. DOI: 10.1029/WR015i002p00489.

Ferro, C.A.T., Segers, J., 2003. Inference for clusters of extreme values. Journal of the Royal Statistical Society. Series B: Statistical Methodology, 65 (2), pp. 545-556. DOI: 10.1111/1467-9868.00401.

Leadbetter, M. R. (1983) Extremes and local dependence in stationary sequences. chrift für Wahrscheinlichkeitstheorie und Verwandte Gebiete, 65, 291–306. DOI: 10.1007/BF00532484.

Viselli, A.M., Forristall, G.Z., Pearce, B.R., Dagher, H.J., 2015. Estimation of extreme wave and wind design parameters for offshore wind turbines in the Gulf of Maine using a POT method. Ocean Engineering, 104, pp. 649-658. DOI: 10.1016/j.oceaneng.2015.04.086.

Arns, A., Wahl, T., Haigh, I.D., Jensen, J., Pattiaratchi, C., 2013. Estimating extreme water level probabilities: a comparison of the direct methods and recommendations for best practise. Coastal Engineering, 81, pp. 51-66. DOI: 10.1016/j.coastaleng.2013.07.003.

Sartini, L., Mentaschi, L. and Besio, G., 2015b. Comparing different extreme wave analysis models for wave climate assessment along the italian coast. Coastal Engineering, 100: 37-47.

Méndez, F.J., Menéndez, M., Luceño, A., Losada, I.J., 2006. Estimation of the long-term variability of extreme significant wave height using a time-dependent Peak Over Threshold (POT) model. Journal of Geophysical Research: Oceans, 111, 7. DOI: 10.1029/2005JC003344.

Luceño, A., Menéndez, M., Méndez, F.J., 2006. The effect of temporal dependence on the estimation of the frequency of extreme ocean climate events. Proceedings of the Royal Society A: Mathematical, Physical and Engineering Sciences, 462, pp. 1683-1697. DOI: 10.1098/rspa.2005.1652.

Stephenson, A. and Tawn, J., 2004. Bayesian inference for extremes: Accounting for the three extremal types. Extremes, 7, pp. 291-307. DOI: 10.1007/s10687-004-3479-6.

Coles, S., Powell, E., 1996. Bayesian methods in extreme value modelling: A review and new developments. International Statistical Review 64, 119–136. DOI: 10.2307/1403426.

Braak, C.J.F.T., 2006. A Markov chain Montecarlo version of the genetic algorithm differential evolution: Easy bayesian computing for real parameter spaces. Statistics and Computing, 16, pp. 239-249. DOI: 10.1007/s11222-006-8769

Gelman, A., Shirley, K., 2011. Inference from Simulations and Monitoring Convergence in Handbook of Markov Chain Monte Carlo. Chapman & Hall/CRC. DOI: 10.1111/j.1751-5823.2011.00179 9.x

Scotto, M.G. and Guedes Soares, C., 2007. Bayesian inference for long-term prediction of significant wave height. Coastal Engineering, 54, pp. 393-400. DOI: 10.1016/j.coastaleng.2006.11.003.

Gibson, R., 2011. A hierarchical Bayesian spatial directional model for wave heights and structural response. Proceeding of the 12th International workshop on wave hindcasting and forecasting, World Meteorological Organization. Hawai, 2011.

Antonini, A., Archetti, R., Lamberti, A., 2017. Wave simulation for the design of an innovative quay wall: The case of Vlorë Harbour. Natural Hazards and Earth System Sciences, 17, pp. 127-142. DOI: 10.5194/nhess-17-127-2017.

Schweizer, J., Antonini, A., Govoni, L., Gottardi, G., Archetti, R., Supino, E., Berretta, C., Casadei, C., Ozzi, C., 2016. Investigating the potential and feasibility of an offshore wind farm in the Northern Adriatic Sea. Applied Energy, 177, pp. 449-463. DOI: 10.1016/j.apenergy.2016.05.114.

Det Norske Veritas, 2010. Recommended Practice DNV-RP-C205, Environmental Conditions and Environmental Loads.

Trinh, Q., Raby, A., Banfi, D., Corrado, M., Chiaia, B., Rafiq, Y., Cali, F., 2016. Modellig the Eddystone Lighthouse response to wave loading. Engineering Structures, 125, pp. 566-578. DOI: 10.1016/j.engstruct.2016.06.027.

Brownjohn, J.M.W., Raby, A., Bassitt, J., Antonini, A., Hudson, E., Dobson, P., 2018. Experimental modal analysis of British rock lighthouses. Marine Structures 62, pp. 1-22. DOI: 10.1016/j.marstruc.2018.07.001.

Met éireann, 2019. The Irish Meteorological Service web site, https://www.met.ie/# . [accessed: 06/02/2019]

Peeters, B. and De Roeck, G., 2001a. Stochastic System Identification for Operational Modal Analysis: A Review. ASME. Journal of Dynamic Systems, Measurement, and Control 123 (4), pp. 659-667. doi:10.1115/1.1410370.

Brownjohn, J.M.W., Hao, H., Pan, T.C., 2001. Assessment of structural condition of bridges by dynamic measurements. Applied Research Project RG5/97, NTU School of CSE, Singapore, April, 2001.

Brownjohn, J., F. Magalhaes, E. Caetano, and A. Cunha, 2010. Ambient vibration re-testing and operational modal analysis of the Humber Bridge. Engineering Structures, vol. 32, pp. 2003–2018. DOI: 10.1016/j.engstruct.2010.02.034.

Peeters, B., De Roeck, G., 2001b. One-year monitoring of the Z24-Bridge: environmental effects versus damage events. Earthquake Engineering & Structural Dynamics, 30, pp. 149–171. DOI: 10.1002/1096-9845(200102)30:2<149::AID-EQE1>3.0.CO;2-Z.

Liu, Y.-C., Loh, C.-H., Ni, Y.-Q., 2013. Stochastic subspace identification for output-only modal analysis: Application to super high-rise tower under abnormal loading condition. Earthquake Engineering and Structural Dynamics, 42 (4), pp. 477-498. DOI: 10.1002/eqe.2223.

Lee, S.Y., Huynh, T.C., Kim, J.T., 2018. A practical scheme of vibration monitoring and modal analysis for caisson breakwater. Coastal Engineering, 137, pp. 109-119. DOI:10.1016/j.coastaleng.2018.03.008

Welch, P., 1967. The use of fast Fourier transform for the estimation of power spectra: A method based on

Richardson, M.H. and Formenti, D.L., 1985. Global curve fitting of frequency response measurements using rational fraction polynomial method. Proc. 3rd International Modal Analysis Conference, Orlando (U.S.A.).

Watson, J., 1911. British and foreign building stones. Cambridge: Cambridge University Press.

Pappas, A., D'Ayala, D., Antonini, A., Brownjohn, J., & Raby, A., 2017. Numerical modelling of Fastnet lighthouse based on experimental dynamic identification. In International Conference on Advances in Construction Materials and Systems ICACMS-2017. Chennai.

Goda, Y., Haranaka, S., Kitahata, M., 1966. Study on impulsive breaking wave forces on piles. Report Port and Harbour Technical Research Institute 6 (5), 1– 30, (in Japanese).

Abaqus. (2014). Abaqus documentation - version 6.14, Dassault Systèmes, Providence, RI, USA.

Pappas, A., D'Ayala, D., Antonini, A., Raby, A., 2019. Finite Element Modelling and Limit Analysis of Fastnet Lighthouse Under Impulsive Ocean Waves. RILEM Bookseries, 18, pp. 881-890. DOI: 10.1007/978-3-319-99441-3_95.

Antonini et al.: SURVIVABILITY ASSESSMENT OF FASTNET LIGHTHOUSE

Highlights

- Bayesian extreme values analysis is applied to 27 years of wave hindcast data in order to describe the extreme wave climate off the Fastnet rock;

- Prior informative distributions for the shape and scale parameters are defined from the data coming from the surrounding numerical nodes;

- The breaking wave load is defined on the basis of previously published methods without the use of any numerical simulations or physical modelling;

- Field modal analysis is performed in order to identify dynamic parameters of the lighthouse as well as to provide real data for the validation of the structural numerical model;

- For the first time, a discontinuous finite element model is applied to the analysis of the coastal structures;

- The survivability of the historic Fastnet lighthouse is performed on the basis of the validated numerical model, being subjected to a breaking wave load arising from the 250 year return period wave.